Preprints.org

Article

Not peer-reviewed version

Characteristics of Cu-Au-Bearing Quartz Veins at Danyore Valley Area, Kohistan Terrane, Northern Pakistan: Evidence from Geological, Geochemical, and Geochronological Studies

Iqtidar Hussain , Huan Li * , Mohamed Faisal , Muhammad Naseer , Jianqi Zhou , Hasnain Ali , Massam Ali

Posted Date: 13 May 2024

doi: 10.20944/preprints202405.0851.v1

Keywords: Cu-Au mineralization; Quartz veins; U-Pb zircon dating; Danyore Valley; Kohistan Batholith; Northern Pakistan

Preprints.org is a free multidiscipline platform providing preprint service that is dedicated to making early versions of research outputs permanently available and citable. Preprints posted at Preprints.org appear in Web of Science, Crossref, Google Scholar, Scilit, Europe PMC.

Copyright: This is an open access article distributed under the Creative Commons Attribution License which permits unrestricted use, distribution, and reproduction in any medium, provided the original work is properly cited.

Preprints.org (www.preprints.org) | NOT PEER-REVIEWED | Posted: 13 May 2024 doi:10.20944/preprints202405.0851.v1

Disclaimer/Publisher's Note: The statements, opinions, and data contained in all publications are solely those of the individual author(s) and contributor(s) and not of MDPI and/or the editor(s). MDPI and/or the editor(s) disclaim responsibility for any injury to people or property resulting from any ideas, methods, instructions, or products referred to in the content.

Article

Characteristics of Cu-Au-Bearing Quartz Veins at Danyore Valley Area, Kohistan Terrane, Northern Pakistan: Evidence from Geological, Geochemical, and Geochronological Studies

Iqtidar Hussain [1], Huan Li [1,*], Mohamed Faisal [1,2], Naseer Kakar [1], Jianqi Zhou [1], Hasnain Ali [3] and Massam Ali [4]

[1] Key Laboratory of Metallogenic Prediction of Nonferrous Metals and Geological Environment Monitoring, Ministry of Education, School of Geosciences and Info-Physics, Central South University, Changsha 410083, China
[2] Department of Geology, Faculty of Science, Suez Canal University, El-Ismailia 41522, Egypt
[3] Key Laboratory of Mineral Resources in Western China, School of Earth Sciences, Lanzhou University, Lanzhou 730000, China
[4] State Key Laboratory of Ore Deposit Geochemistry, Institute of Geochemistry, Chinese Academy of Sciences, Guiyang 550081, China
* Correspondence: lihuan@csu.edu.cn

Abstract: Danyore Valley area is a new prospect of copper-gold mineralization in the Gilgit-Baltistan province, Kohistan terrane, northern Pakistan. The mineralization is Cu-Au vein-type, localized within quartz veins and controlled by a fracture system mainly trending NW and NE. The host units belong to the Ladakh-Kohistan arc terrane, which covers northern Pakistan and north-western India and mainly comprises Precambrian basement units, Paleozoic to Cenozoic magmatic rocks, and sedimentary strata. The mineralized wall rocks consist of Mesozoic gabbro and diorite, which have undergone an intensive hydrothermal alteration. The study area, Danyore Valley, has yet to be explored. The geological background and mineralization type in literature are scarce. Moreover, the tectonic setting, petrogenesis, age, and magmatic evolution of the gabbro-diorite hosting unit still need to be better understood. Furthermore, the sources of metals and mineralized fluids and the types of mineralization and alteration are also unexplored. This research's contribution presents the field investigation, microscopic observations, whole rock geochemistry (major, trace, and REE), mineral analysis (EPMA), in situ LA–ICP–MS zircon U–Pb age dating, and zircon trace elements data for Danyore Valley Cu-Au prospect of Kohistan Batholith. The current research work's objectives are to (a) constrain the emplacement ages of the Danyore Valley host rocks, (b) determine the petrogenesis and tectonic environment of the gabbro-diorite wall rocks, and (c) identify the mineralization style and alteration patterns of Cu-Au occurrences. The U-Pb isotopic data of studied zircons from Danyore Valley diorite specimens yielded concordia ages from 111.60 ± 0.90 Ma to 112.18 ± 0.74 Ma. Correspondingly, the gabbro rock sample displayed a concordia age of 110.21 ± 0.99 Ma, indicating the crystallization time of the host bodies is mainly the early cretaceous period (~110 Ma). The findings of this study reveal that the calc-alkaline affinity and arc-like geochemical characteristics of the gabbro and diorite rocks have been characterized by a significant enrichment in large-ion lithophile elements and an apparent depletion in high-field strength elements. The parent magma probably originated from a partial melting process of mantle depletion, and geochemical traits are characteristic of magmas associated with subduction zones. The Danyore Valley area of Kohistan terrane is defined by the existence of several mineralized quartz veins, which are mainly sulfide assemblages. The sulfide ore is mainly comprised of chalcopyrite, pyrite, and bornite, with a smaller amount of covellite and sphalerite and significant traces of gold, which are distributed mainly in sulfides. Copper and gold mineralization of Danyore Valley is associated with phyllic, propylitic, and carbonatization alteration assemblages. Metal-rich quartz veins exhibit a spatial correlation with diorite and gabbro rocks. The discovery of several surface Cu-Au vein-type mineralized areas accompanying outcrops of copper supergene

© 2024 by the author(s). Distributed under a Creative Commons CC BY license.

Preprints.org (www.preprints.org) | NOT PEER-REVIEWED | Posted: 13 May 2024 doi:10.20944/preprints202405.0851.v1

enrichment at the Danyore Valley prospect is significant evidence (predictor patterns) of porphyry-style deposits in the Gilgit district, Kohistan terrane, northern Pakistan. This work also advocates the importance of the Danyore Valley prospect and Kohistan Batholith region for further detailed geological studies.

Keywords: Cu-Au mineralization; quartz veins; U-Pb zircon dating; Danyore Valley; Kohistan Batholith; Northern Pakistan

1. Introduction

Gold and copper association is reported in several ore deposits worldwide, including porphyry-style ore deposits, Iron Oxide Copper-Gold (IOCG) deposits, epithermal deposits, orogenic gold deposits, skarn deposits, and Volcanogenic Massive Sulfide (VMS) deposits. Porphyry-type deposits are one of the largest gold-copper reservoirs in the upper crust, accounting for over 100 tons of Au and 50% of the global copper resource reserves. These copper deposits primarily originated from low-temperature magmatic-hydrothermal fluids at shallow levels (<5 km depth) in continental and island-arc orogenic settings. It is generally acknowledged that gold can be removed from the porphyry–epithermal system by later hydrothermal fluids, which form Cu-Au-rich quartz veins surrounding the felsic intrusion bodies (Chiaradia, 2020; Garwin, 2019; Hou and Cook, 2009; Kerrich et al., 2000; Kesler et al., 2002; Sillitoe, 2010). Secondary copper staining (malachite, azurite, and chrysocolla minerals) and alteration assemblages (potassic, phyllic, argillic, and propylitic) in bedrock exposures are frequently observed in the vicinity of hydrothermal deposits; they are valuable indicators for prospecting (Ma et al., 2021; Raza et al., 2021; Zhang et al., 2019; Zhao et al., 2021).

Global geologists have collaborated for over a half-century to significantly advance our knowledge of geodynamic mechanisms and ore formation in various tectonic settings, including intraplate regions, continental rifts, and accretionary orogens (Arndt et al., 2005; Candela and Piccoli, 2005; Franklin et al., 2005; Goldfarb et al., 2005; Kerrich et al., 2005). However, a better comprehension of the metallogenesis of orogens originating from continent-to-continent collisions is needed; the formation of numerous giant deposits still needs to be more adequately understood. The surface of the Earth is known for having several mountain belts that formed during the collision of continents, such as the Variscan orogen in Western and Central Europe (Seltmann et al., 1994; Sibuet et al., 2004; Zhang, 1997), the Himalayan-Tibetan orogen in Asia (Yin et al., 2000).

The Himalayan-Tibetan orogen contains many hydrothermal-magmatic ore deposits (i.e., Pb-Zn deposits, porphyry copper deposits, orogenic Au deposits, Sn–W deposits.) (Seltmann et al., 1994; Yin et al., 2000; Zaw et al., 2007). It mainly comprises the Karakorum and Himalayas ranges in the south and the Tibetan plateau in the north. It involves several terranes such as Eastern kunlun-qaidam area, Ladakh-Kohistan arc terrane, Songpan-Ganzi-Hoh area, Qiangtang Terrane (500–600 km wide), and Lhasa Terrane (300 km wide) (Yin et al., 2000).

Ladakh-Kohistan arc terrane covers northern Pakistan and north-western India and is mostly composed of Precambrian basement units, Paleozoic to Cenozoic magmatic rocks, and sedimentary strata (Figure 1). Numerous geological, geochemical, and isotope studies (Miandad et al., 2014; Shah et al., 2012) had been carried out in the Kohistan terrane of northern Pakistan and several ore deposits and mineral occurrences were discovered, such as Copper-lead polymetallic veins deposits (Hussain et al., 2021; Hussain et al., 2023), rare earth elements (REE) mineralization in alkaline rocks (Hussain et al., 2020), placer gold deposits adjacent to the Indus River and its tributaries (Alam et al., 2019).

The Danyore Valley area is located in the Gilgit district at the central part of the Kohistan terrane (Figure 2). It is mainly covered by intrusive granitoid rocks of the Kohistan Batholith. Systematic geological studies relating to the geochemistry of granitoids and their tectonic settings are lacking in the literature. During our field investigations, large surface exposures of green-blue secondary copper stains were found in many places within the gabbro-diorite intrusion bodies of the Kohistan Batholith. In addition, significant hydrothermal quartz veins are recorded for the first time in the

Preprints.org (www.preprints.org) | NOT PEER-REVIEWED | Posted: 13 May 2024 doi:10.20944/preprints202405.0851.v1

Danyore Valley prospect. These veins are characterized by Cu-Au-rich sulfide minerals, surrounded by pervasive alterations. Due to the lack of advanced geochemical data and isotope analyses, the characteristics of hydrothermal metallic ore veins and the geochemical signatures, age, and tectonic setting of the host granitoids are poorly understood. Selected samples were taken from gabbro, diorite host rock outcrops, and metal-bearing quartz veins. The intended outcomes of this research are (a) to constrain the age, tectonic setting, and petrogenesis of the wall rock units, (b) to identify the mineralization style and alteration patterns, and (c) to establish a magmatic-hydrothermal model for the area. In order to achieve the objectives of this work, fieldwork, microscopic observations, whole rock geochemistry (major, trace, and rare earth elements), mineral analysis, LA–ICP–MS zircon U–Pb age dating, and zircon trace elements are conducted to the collected samples from the Danyore Valley Cu-Au prospect. The findings of this study address an enormous research gap relating to the Mesozoic magmatism of the Kohistan Batholith and suggest that the Danyore Valley prospect is a potential porphyry-style/vein-type hydrothermal Cu-Au mineralization, which indicates that further geological and geochemical prospecting research is needed.

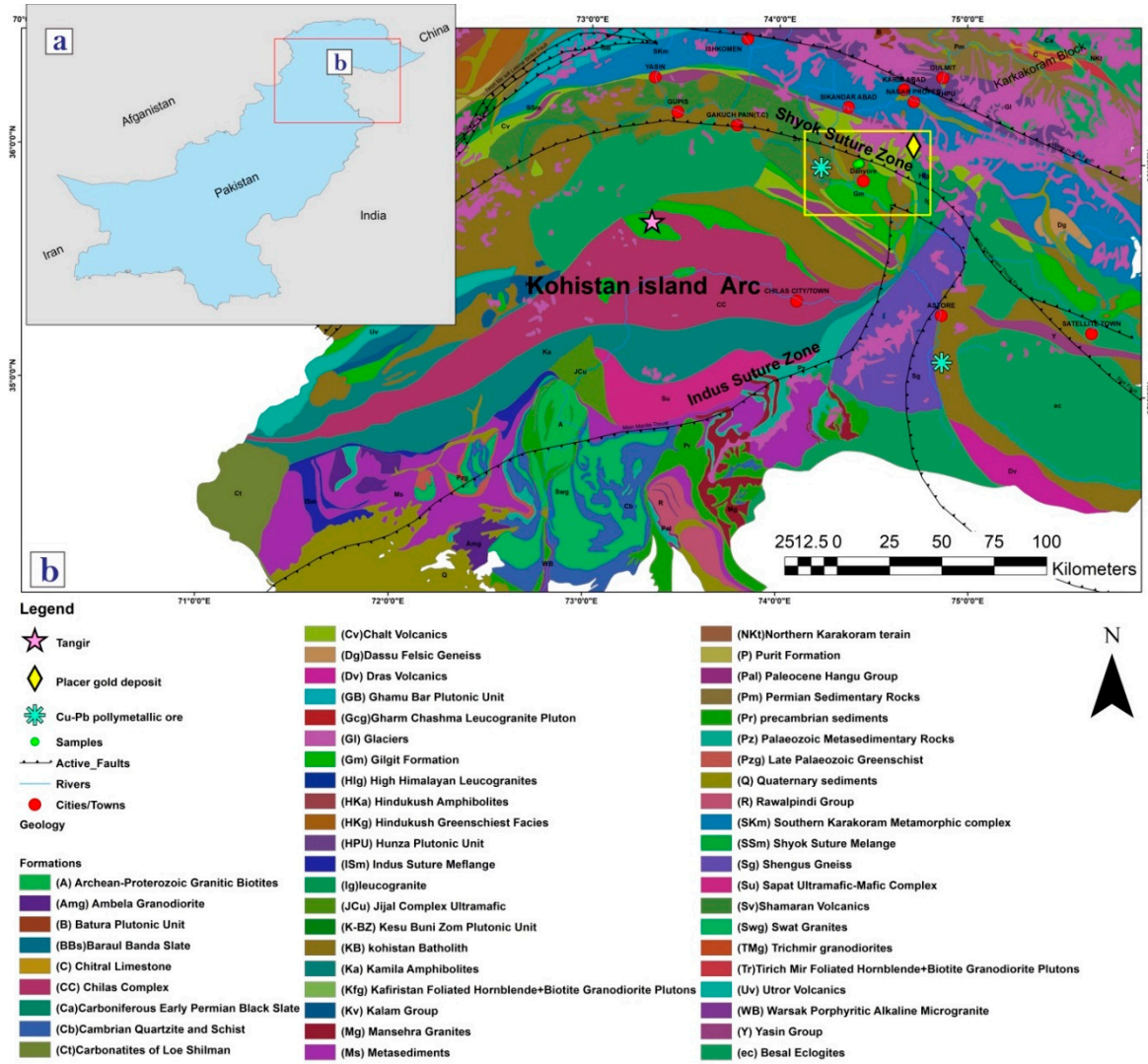

Figure 1. (a) A regional map showing the location of Pakistan; (b) a general geological map showing the primary lithological units and tectonic zones in Northern Pakistan, modified after (Zanchi et al., 2011).

Preprints.org (www.preprints.org) | NOT PEER-REVIEWED | Posted: 13 May 2024 doi:10.20944/preprints202405.0851.v1

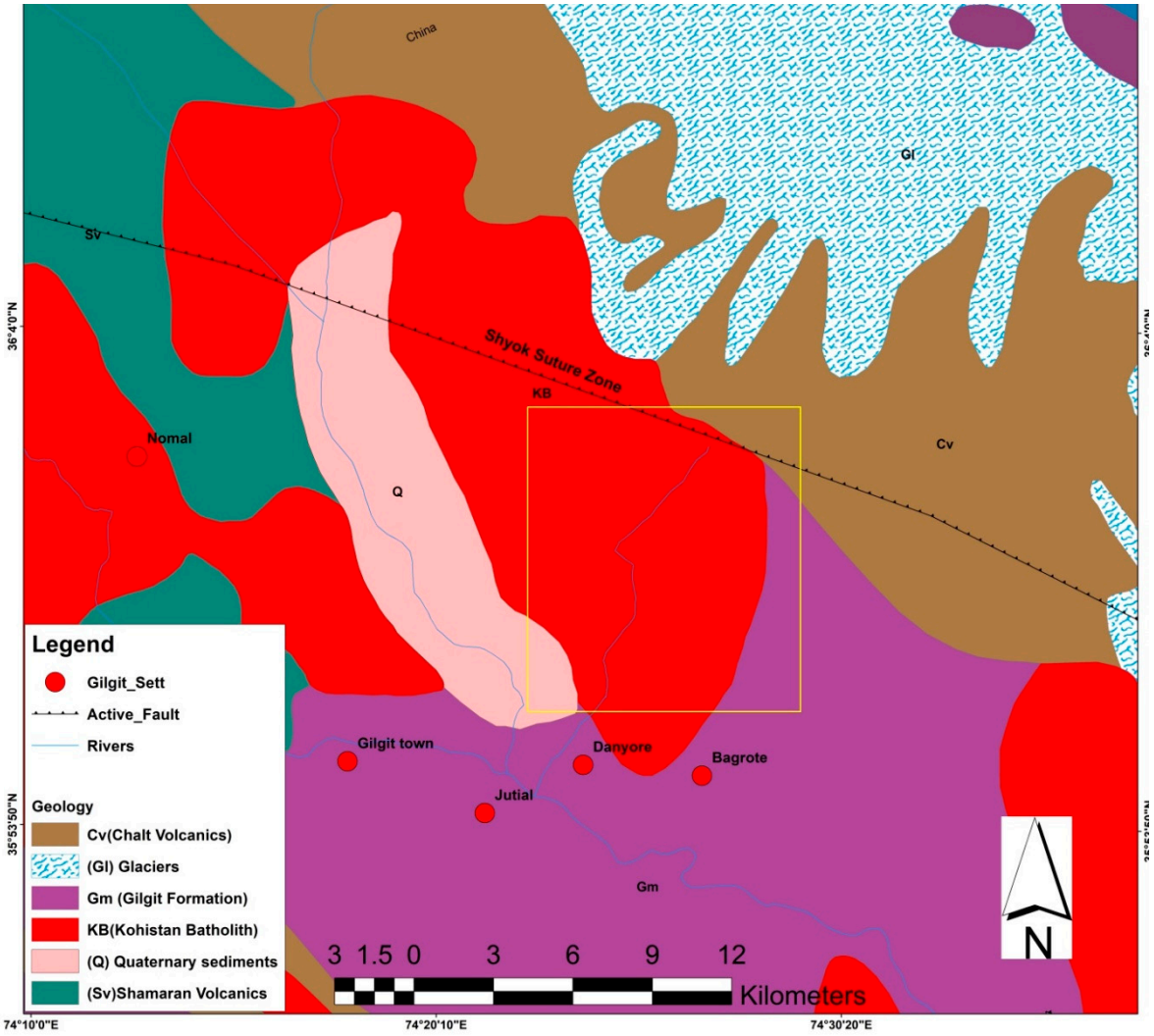

Figure 2. A simplified geological map of the Danyore Valley area and its nearby surroundings, Northern Pakistan, modified after (Zanchi et al., 2011).

2. Geological Background

2.1. Regional Geology

Pakistan has a prominent position in the field of geology owing to its diverse geological features. It encompasses three significant tectonic plates, namely the Eurasian, Indian, and Arabian plates (Molnar et al., 1975). Numerous ore deposits have been documented within the Tethys domain (Figure 1a). These include the porphyry copper (Cu) and gold (Au) deposits in Chaghi and Rekodeq, placer gold deposits in northern areas (Alam et al., 2023); gold (Au) mineralization attributed to sulfide occurrences in the Chitral region known as Awireth-Krinj (Ahmad et al., 2018) and veins-type gold (Au) deposits in the Artsan area of Chitral (Calkins et al., 1981).

The geological formations across Pakistan exhibit considerable variations from one region to another, displaying different rock types that span various ages. During the pre-Cretaceous era, approximately 110 million years ago, the Indian landmass was still undergoing significant tectonic activity, exhibiting geological folding alongside the African continent. According to several studies (Bignold, 2003; Coward et al., 1987; Khan et al., 1993; Searle et al., 1987), a collision/obduction between the Asian and Indian plates happened in the Early Tertiary and Late Cretaceous periods (with the Indian continent at ~60–50 Ma; with the Eurasian continent at 54–34 Ma). Jagoutz et al. (2009) stated that the calc-alkaline Matum Das intrusion indicates the initial stage of subduction. During the Late Cenozoic period (~45 Ma), the Eurasian and Indian plates encountered, forming substantial

Preprints.org (www.preprints.org) | NOT PEER-REVIEWED | Posted: 13 May 2024 doi:10.20944/preprints202405.0851.v1

mountain chains, such as Karakorum, Hindukush, and Himalayan ranges (Kazmi and Jan, 1997). Two volcanic arc belts are present in north Pakistan, namely the Chaghi and Kohistan arc belts (Bukhari et al., 2010). The Tethyan suture zones of the Himalayas (Figure 1) were used to divide the north Pakistan region into three major blocks: the Karakoram block, the Indo-Pakistan plate, and the Kohistan island arc block (Robertson and Collins, 2002).

The Karakoram block originated in the late Permian–Triassic period on the southern margin of the Asian tectonic plate. The Karakorum Fault separates the Karakorum block from southern Tibet (Zanchi et al., 2011). The major constituents of the Karakoram Block are high-grade metamorphic rocks, consisting mainly of dolomitic marbles, clinopyroxene amphibolites, interlayered sillimanite-grade pelites, and kyanite with garnet (Rolland et al., 2009).

The Indo-Pakistan plate's interaction with the Asian plate triggered the stress, which resulted in the subduction of the Tethys oceanic crust along the Karakoram Suture, which led to the formation of the Karakoram Range. Subsequent stress events caused the Tethys sea plate to subduct under the Kohistan-Ladakh belt alongside the Northern Indus Suture, leading to the formation of the Kohistan-Ladakh magmatic arc (Petterson et al., 1985; Searle et al., 1987; Tahirkheli, 1979). At approximately 68 Ma, the Indo-Pakistan tectonic plate and the Afghan block preliminary were encountered during the Late Cretaceous period. Also, the Indus suture has experienced significant development through the obduction of ophiolites (Malkani et al., 2019).

Kohistan Island Arc block (also called Kohistan terrane or Kohistan complex, Figure 1) is surrounded by Afghanistan to the west, China to the north, and India to the east (Virdi, 1987). The island arc of this terrane is formed during the Cretaceous time (approximately during the period from 120 to 80 Ma) resulting from the intraoceanic diminution (Neo-Tethys ocean) (Shah and Shervais, 1999). The Kohistan Island Arc is situated within north of Pakistan, particularly in the Kohistan region, and continues into the parts of Gilgit-Baltistan and is parted from the Asian plate by the main Karakorum thrust fault (Shyok suture zone) (Jan and Tahirkheli, 1979), and from the Indian plate by main mantle thrust fault (Indus suture zone) (Petterson et al., 1985; Searle et al., 1999). Generally, the Kohistan region is often categorized into three main complexes: Giligit Complex, Chilas Complex, and Southern Plutonic Complex.

2.1.1. Gilgit Complex

(a) Volcano-sedimentary succession includes Teru/Shamaran Volcanic Formation and Dir Volcanics Group. Teru/Shamaran Volcanic is composed of rhyolites, ignimbrites, and volcaniclastics (silicic) found discordantly on a batholith-volcanic basement. The Dir Volcanics has two sections: the bottom one is chiefly comprised of turbiditic sandstones and siltstones with small limestone outcrops, while the upper part has volcanic breccias, sandstones, mudstones, ignimbrites, and rhyolites which have been trespassed by the younger Utror volcanics (Danishwar et al., 2001; Shah and Shervais, 1999; Sullivan, 1992; Tahirkheli, 1979).

(b) Yasin sedimentary Group has several exposures of volcanic sets, consisting of agglomerates, tuffs, and lavas. They principally contain patches of fossiliferous, massive, and shaly limestones. Sandstone layers are also found in some places. Based on the evidence from sedimentary sequences, the sedimentary layers of the Yasin Group were probably deposited during the Aptian-Albian age (i.e., early Cretaceous time) when the intra-oceanic Kohistan island arc was formed (Pudsey, 1986; Tahirkheli and Jan, 1984).

(c) Kohistan Batholith is characterized by intraoceanic and continental magmatism with ages ranging from 112–42 Ma. This huge igneous body intruded into the Juglot and Chalt Volcanic Group to the north and south. Kohistan batholith contains multiple types of lithologies, mainly plutonic rocks consisting of granites, diorite, gabbroic diorite, and gabbroic (Bignold et al., 2006; Coward et al., 1987; Petterson et al., 1985)

2.1.2. Chilas Complex

The Chilas complex is an extensive exposure of intrusive body (Hamidullah and Jan, 1986; Khan et al., 1993), primarily calc-alkaline plutonic rocks with composition ranging from mafic to ultramafic

Preprints.org (www.preprints.org) | NOT PEER-REVIEWED | Posted: 13 May 2024 doi:10.20944/preprints202405.0851.v1

(Bignold et al., 2006). Diorites and gabbronorites dominate the complex, while gabbros, mafic dykes, troctolites, peridotite, anorthosite, and dunites constitute minor components (Khan Tehseenullah et al., 1996). This complex's ages ranged between 84+0.5 Ma of U–Pb zircon age dating (Zeitler and Chamberlain, 1991) and 69.5+9.3 Ma of Sm-Nd isotope dating (Yamamoto and Nakamura, 2000).

2.1.3. Southern Plutonic Complex

(a) Jijal complex: It consists of ultramafic rocks, including harzburgites, websterites, dunites, norites, pyroxenites, garnet granulites, amphibolites, and hornblendites (Jan and Howie, 1981; Tahirkheli et al., 2012). These rock units ages range from 91.8+1.4 Ma (U–Pb zircon dating) (Schaltegger et al., 2002) to 117+7 Ma (Sm-Nd isotopes analysis) (Dhuime et al., 2007).

(b) Kamila Amphibolite: the amphibolite from this rock unit is chiefly composed of plutonic rocks (diorites, gabbros and norites) and metavolcanic (mostly basaltic andesites and basalts). Other lithologies are granites, tonalites, diorites, garnet quartzites and calc-silicates, anorthosites, hornblendites, and hornblende schists (Jan, 1990; Shah and Shervais, 1999). According to Anczkiewicz (2000), the age of the Kamila Amphibolite is 95 to 100 Ma.

2.2. Local Geology

The Kohistan Batholith is a main intrusive complex in northern Pakistan (Figure 1b), forming part of the Trans-Himalayan Batholith. Kohistan Batholith spans approximately two hundred and seventy kilometers from west to east. The batholith covers 168 miles from its eastern extent, starting with the Nanga Parbat Haramosh Massive (NPHM) and extending westward to the Shyok Suture Zone (SSZ). Additionally, it has a width of 34 miles and a north-south dimension ranging from 50 to 60 km, making up a substantial portion of the twenty seven hundred kilometers long Trans-Himalayan Batholith (THB) (Petterson et al., 1985).

The Kohistan Batholith developed in four major magmatic phases: (a) the first phase is composed of foliated gabbro-diorites, Matum Das tonalite, and deformed intrusive rocks of 102 Ma; (b) the second event undeformed gabbros and gabbro-diorites igneous bodies which were generated around 80-60 Ma; (c) the third stage emplaces granites and granodiorites with the age of 60-40 Ma, (d) the younger phase includes granite and leucogranite sheets which formed around 50-24 Ma (Bignold et al., 2006; Heuberger et al., 2007; Petterson et al., 1985; Treloar et al., 1989). Most of these intrusions are volumetric plutons ranging from modest to massive, with significant vertical and horizontal orientation, with several dikes, sills, sheets, and lopoliths also reported (Khan et al., 1998; Khan Tehseenullah et al., 1996; Treloar et al., 1996).

The Danyore Valley area lies in the Gilgit district, within the Kohistan plutonic Batholith of the Kohistan Arc belt (Figure 2). It is situated approximately 13 kilometers northwest of Gilgit City (Northern Pakistan) (Figure 3). Chilas is positioned southwest of the research area, while Utror and Chalt (also known as Dir, Shamran, Juglot, and Yasin) are situated in the north side of research (Khan et al., 1993). Geological characteristics of the research area include gabbro, gabbro-diorite, diorite, and granite bodies. The collected hand specimens from these rock units display that the mineral assemblages are dominantly massive, medium to coarse-grained quartz, plagioclase, mica, potash feldspar, and calcite (Figures 3 and 4).

During the current research investigation, the outcrops of gabbro and diorite bodies (Figure 4a–c) generally exhibit a greenish-to-blue shade due to the presence of minerals that contain copper, primarily malachite and azurite. On the surface, which can easily be identified on hand specimens (Figure 4d–h). Furthermore, Cu-Au occurrences have been recognized for the first time in many places within the study area. The mineralization mainly comprises a stockwork of fractures, veins, and veinlets with NW and NE orientations (Figure 4c). The host rocks display features like silicification and biotite alterations, and they are essentially related to the presence of mineralized quartz veins.

Preprints.org (www.preprints.org) | NOT PEER-REVIEWED | Posted: 13 May 2024 doi:10.20944/preprints202405.0851.v1

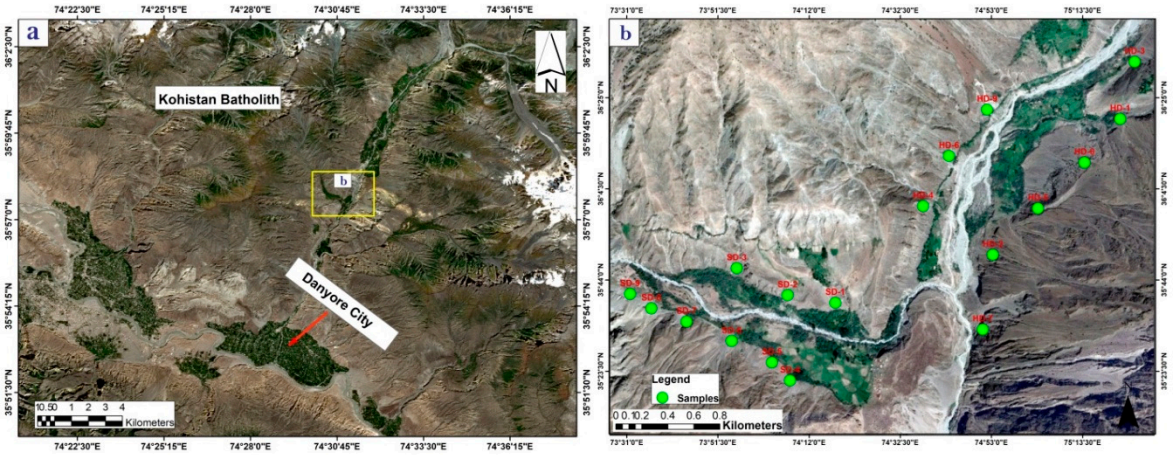

Figure 3. Landsat images for the study area (Danyore Valley, Kohistan Batholith, Northern Pakistan) and (b) locations of the collected samples.

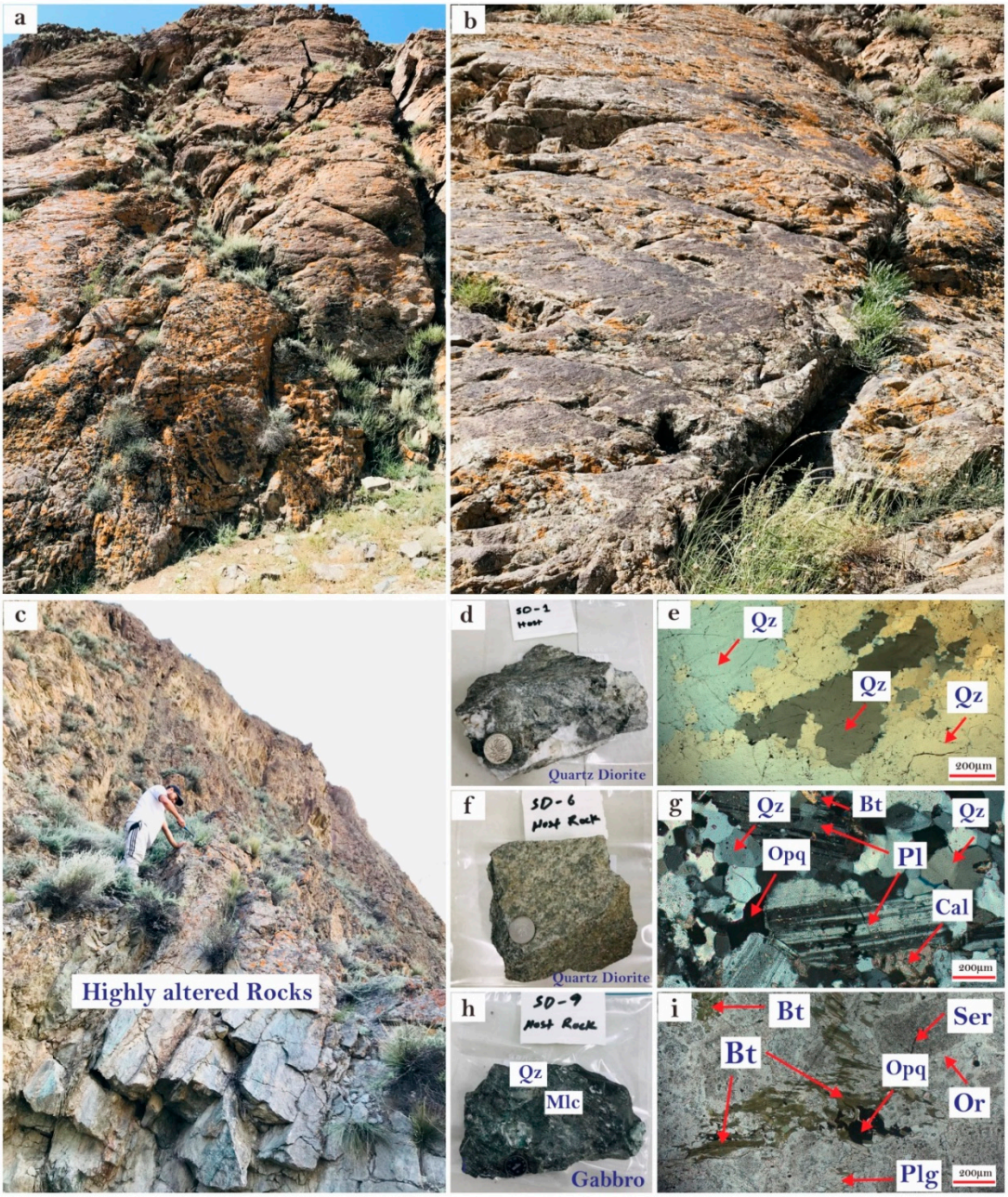

Preprints.org (www.preprints.org) | NOT PEER-REVIEWED | Posted: 13 May 2024 doi:10.20944/preprints202405.0851.v1

Figure 4. Field photographs, hand specimens, and microphotographs of Danyore Valley copper-gold prospect, Northern Pakistan: (a-c) close-up view of the highly altered outcrops of the host rock; (d-e) fine-grained diorite wall rock (sample SD-1) which rich mainly in quartz grains (XPL); (f-g) medium-grained diorite (sample SD-6) showing plagioclase crystals (undergone sericite alteration), quartz, biotite, and abundant calcites (XPL); (h) hand specimen of gabbro host rock (sample SD-9) slightly covered by malachite of secondary supergene enrichment, (i) microphotograph of gabbro display the essential minerals such as plagioclase (highly altered to sericite) and biotite with dark and opaque minerals (malachite and sulfide) (PPL). Abbreviations: Qz (Quartz), Bt (Biotite), Pl (Plagioclase), Or (Orthoclase), Cal (Calcite), Opq (Opaque), Mlc (Malachite), Ser (Sericite),), XPL (Crossed polarized light), PPL (Plain polarized light).

2.2.1. Petrography Characteristics of the Host Units

The diorite rocks of the Danyore Valley area consist of essential minerals such as plagioclase (41%), quartz (36%), and biotite (7%), with a minor amount of muscovite (5%). The accessory minerals are mainly represented by epidote (2%), calcite (3%), and opaque (1%) minerals (Figure 4d–g). The coalescence of smaller sub-grains frequently causes the larger quartz grains to show patchy extinction (Figure 4e). The prismatic euhedral crystal grains of plagioclase have lengths of up to 200 μm and widths of 80 μm. They can be identified by lamellar twinning, particularly in the center of crystals, which has substantially changed to sericite and epidote (Figure 4g). Some quartz grains have a strong, barely wavy extinction and are mixed in with elongated calcite grains. Biotites at the edges of quartz grains are primarily medium-grained subhedral to euhedral crystals that form irregularly. This suggests that some alteration may have happened to these rocks after they were formed. Muscovite is anhedral to subhedral and has parallel-oriented crystals, creating the strips. Iron oxides and sulfide minerals are considered as opaque minerals (Figure 4g). They can be spotted within the plagioclase crystals and along the cracks as inclusions.

On the other hand, the petrographic observation of the Danyore Valley gabbro (Figure 4h,i) indicates the presence of plagioclase (44%) and biotite (38%) as major constituents, while some hornblende (8%), muscovite (5%), chlorite and opaque (2%) minerals occur as minor components. The majority of biotite and hornblende completely changed into iron oxides and chlorite. Many plagioclase crystals are partially or entirely altered to sericites and epidotes. Biotite can be observed as small to medium-sized, highly evolved flakes that show prominent light brown to dark brown pleochroism. It is predominantly correlated to opaque minerals, chlorite, and occasionally muscovite. Green to dark green pleochroism can be observed in chlorite. Its close affiliation with biotite indicates that it was formed by alteration. Some biotite grains are partially changed to chlorite, and some are entirely converted to chlorite minerals (Figure 4i). The topotaxial growth of biotite can be observed by the presence of chlorite along cleavages in some of the slightly changed grains. Muscovite tends to appear in flakes and tabular-shaped crystals around the plagioclase and quartz.

3. Sampling and Analytical Methods

A total of 90 samples from wall rocks and sulfide-bearing quartz veins were obtained from the study area (Figure 3) during three field trips (2021-2022). Twenty-five samples were selected for thin sections for petrographic studies, and 17 polished thin sections were selected for ore microscopic investigations and to carry out an electron probe microanalysis (EPMA) analysis. Four samples from the study area (host rocks) and three from the previous study (Heuberger et al., 2007) were selected for whole-rock geochemical analysis. Five samples from the wall rocks were selected for geochronology studies to investigate the age of host units. The supplementary data material (SDM I) provides the analytical methodologies procedures.

Preprints.org (www.preprints.org) | NOT PEER-REVIEWED | Posted: 13 May 2024 doi:10.20944/preprints202405.0851.v1

4. Results

4.1. Zircon U–Pb Geochronology

Laser ablation ICP-MS U-Pb analysis and obtained ages for the studied zircons from the Danyore Valley prospect are presented in the supplementary data table (SDT I). 182 spots were selected during geochronological studies. Forty points were obtained on zircon mineral grains from each diorite specimen (SD-1, SD-5, SD-6, and HD-1) and twenty-two spots from the gabbro sample (SD-9). Cathodoluminescence images (CL; Figure 5) were utilized for point selection for the trace element studies (SDT II) to assess the internal structure and outer appearance (morphology) of the specimens. Generally, zircon grains from studied gabbro and diorite samples are brassy yellow to light yellow and mostly anhedral to subhedral crystals that were fractured amidst the ascending of metamorphism or magma and alteration activity, which causes the zircon breakdown (Ayonta Kenne et al., 2021). CL reveals zircon crystals with sizes ranging from large (>210 μm) to short (<60 μm), displaying prismatic and pyramid shapes. However, no clear concentric zonation is observed, as shown in Figure 5.

In sample SD-1 (Diorite), the zircons display prismatic and pyramidal crystal appearances, which vary from euhedral to subhedral, ranging in size between 90 to 190 μm. The measured axial ratios are 1:1 and 2:2. Some grains have weak growth zoning with darker centres (Figure 5a). For the age analysis, twenty-six zircon spots yielded a concordia age of 111.60 ± 0.90 Ma, with a mean square weighted deviation (MSWD) of 0.41 (Figure 6a). The overall average age for the sample SD-1 is reported as 111.60 ± 0.90 Ma with an MSWD of 0.58 (Figure 6a). The 14 remaining grains, showing mild to moderate discordance were removed from the analysis due to substantial evidence of lead loss and metamictization.

The majority of zircons from sample SD-5 (Diorite) lack distinct zoning, although some have distinct clear zoning, and precise prismatic and pyramidal shapes, while other crystals appear colourless. Their size ranges from 60 to 210 μm, and their shapes are particularly euhedral to subhedral (Figure 5b). Thirty-nine of forty zircon spots recorded a concordia age of 112.18 ± 0.74 Ma (MSWD = 0.17). The sample's cumulative mean age is 111.26 ± 0.72 Ma (MSWD = 0.56; Figure 6b).

In sample SD-6 (Diorite), the presence of fluid or mineral inclusions, alteration, and metamorphism suggested a lack of clear zoning in studied zircon crystals. (Ayonta Kenne et al., 2021). The crystal structures of zircons vary from euhedral to subhedral, ranging in size between 90 to 190 μm, and axial ratios of 1:1 and 2:2 (Figure 5c). Thirty-nine spot analysis reported a concordia age of 111.64 ± 0.73 Ma (MSWD = 0.92). The sample SD-6 total mean age is 111.64 ± 0.73 Ma (MSWD = 0.55; Figure 6c).

The analyzed zircons crystal grains of Sample HD-1 (Diorite) predominantly exhibit a dark colour, while some are colourless. Clear pyramid or prismatic shapes are not easily distinguishable in the cathodoluminescence (CL) micrographs of most zircon crystal in the sample. The zircons have euhedral to subhedral shapes and range in size from 90 to 190 μm (Figure 5d). In terms of the age analysis, the Concordia age of thirty of the forty zircon spots showed 112.17 ± 0.81 Ma (MSWD = 0.072). The sample's average age of this sample is 110.81 ± 0.81 Ma (MSWD = 0.074).

Zircon grains in sample SD-9 (Gabbro) lack clear zoning in CL photographs; most grains appear black. Zircon crystals have a size ranging from 60 to 210 μm. (Figure 5e). During age calculation analysis, twenty zircon analyses yielded a concordia age of 110.21 ± 0.99 Ma (MSWD = 0.98). The sample's mean age is 110.57 ± 0.99 Ma (MSWD = 0.35; Figure 7b).

Preprints.org (www.preprints.org) | NOT PEER-REVIEWED | Posted: 13 May 2024 doi:10.20944/preprints202405.0851.v1

Figure 5. Cathodoluminescence (CL) images of the analyzed zircon grains from the studied samples of Danyore Valley copper-gold prospect, Northern Pakistan. Yellow colored circles show the LA-ICP-MS analysis of the U-Pb dating spot.

Preprints.org (www.preprints.org) | NOT PEER-REVIEWED | Posted: 13 May 2024 doi:10.20944/preprints202405.0851.v1

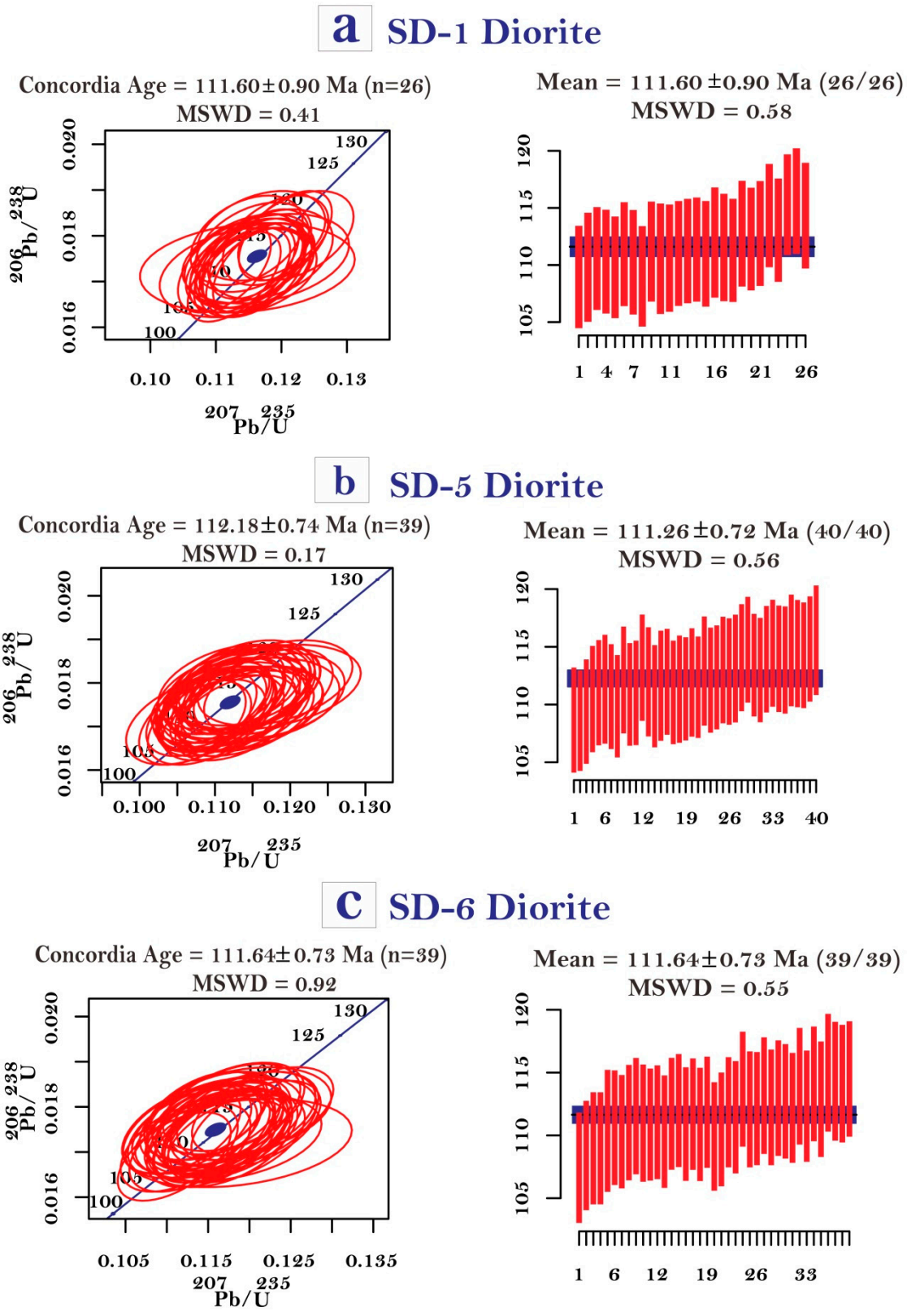

Figure 6. Concordant and weighted mean ages of the studied zircon grains from Danyore Valley copper-gold prospect, Northern Pakistan: (a) sample SD-1 (diorite); (b) sample SD-5 (diorite); (c) sample SD-6 (diorite).

Preprints.org (www.preprints.org) | NOT PEER-REVIEWED | Posted: 13 May 2024 doi:10.20944/preprints202405.0851.v1

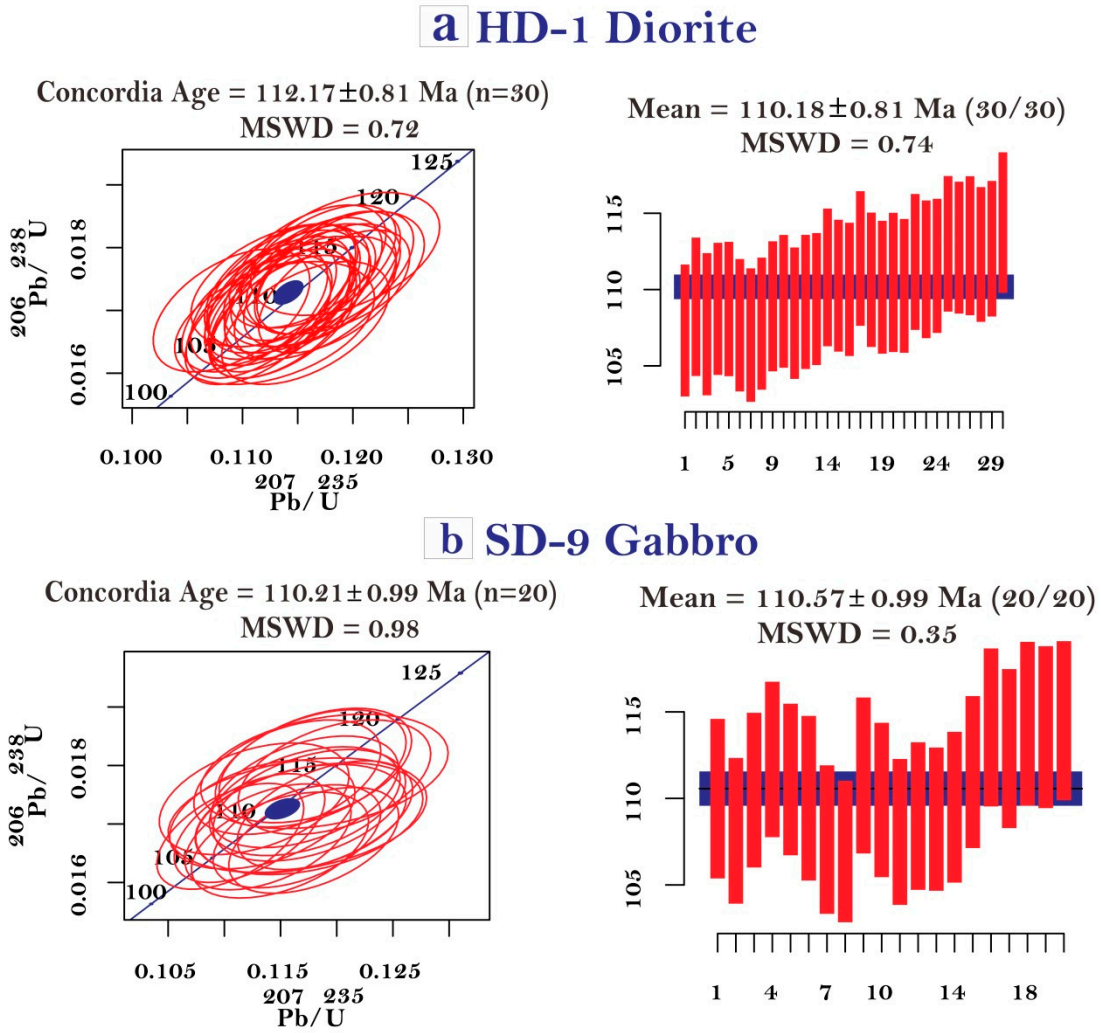

Figure 7. Concordant and weighted mean ages of the studied zircon grains from Danyore Valley copper-gold prospect, Northern Pakistan: (a) sample HD-1 (diorite); (b) sample SD-9 (gabbro).

4.2. Zircon Geochemistry

The results of the trace element analyses (i.e., Y, Nb, Ti, Ta, HF, Pb, U, Th, and REE) are given in SDT (II). The zircons chondrite-normalized REE patterns from the Danyore Valley area of Kohistan Batholith are depleted in HREEs and enriched in LREEs (Figure 8), with prominent positive Ce anomalies and moderate negative Eu anomalies, confirming that the zircons are magmatic (Bao et al., 2014; Hoskin et al., 2003; Rubatto et al., 2017).

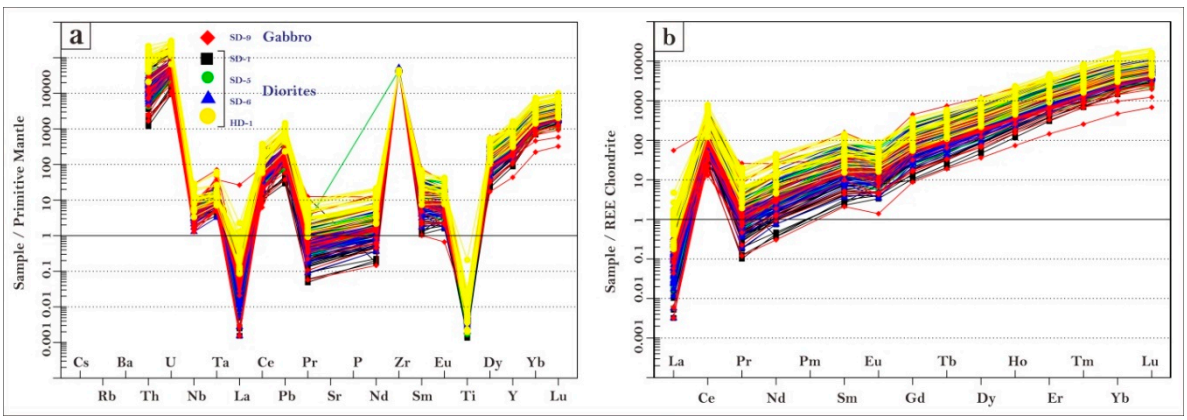

Preprints.org (www.preprints.org) | NOT PEER-REVIEWED | Posted: 13 May 2024 doi:10.20944/preprints202405.0851.v1

Figure 8. (a) Primitive mantle-normalized spider diagram (normalizing values are from (McDonough and Sun, 1995); (b) Chondrite-normalized REE (normalizing values are from (Boynton, 1984)) of studied zircons from Danyore Valley copper-gold prospect, northern Pakistan.

The Eu/Eu* and Ce*/Ce* values for diorite rocks range from 0.22 to 1.51 and 53.89 to 1581.32. For the SD-9 gabbro rock, the values are 0.2 to 0.63 and 4.67 to 640.28, respectively (SDT II). There are profound variations in trace element concentrations within the same sample for zircons. Hafnium values, which are relatively higher in host rocks (diorite and gabbro) samples, range from 4732.78 to 10851.98 ppm, with an average of 7405.99 ppm. Niobium (Nb) and Tantalum (Ta) have a low content in all samples (diorites and gabbro), with abundances ranging from 0.83 to 18.93 ppm (avg. 3.88 ppm) and 0.11 to 2.63 ppm (avg. 0.51).

In summary, the zircon crystals display an extraordinary composition characterized by elevated concentrations of Thorium (Th), Uranium (U), Hafnium, and Yttrium (Y) alongside notably low levels of Tantalum (Ta) and Niobium (Nb). Furthermore, the Th/U ratio of studied grains indicates values of Th/U >1 (SDT II), confirming the magmatic signatures of the studied wall rocks (Hoskin et al., 2003).

4.3. Major, Trace, and Rare Earth Elements (REE)

Four specimens from the current research (one gabbro and three diorites) were chosen for whole-rock geochemical analysis. Additionally, three diorite samples from the previous research (Heuberger et al., 2007) were added to the analysis to assess the potential origin of the parental magma and the tectonic environment of the studied area. The current research's analyzed sample results and relevant geochemical attributes from the reference data (Heuberger et al., 2007), are given in SDT III.

4.3.1. Diorite

The results of major oxides for diorite wall rock display intermediate to a high content of SiO_2 (53.55 to 66.20 wt.%), intermediate to high Al_2O_3 (avg. 17.68 wt.%), Na_2O (avg. 6.14 wt.%), (avg. CaO 2.69 wt.%), (avg. Fe_2O_3 1.88 wt.%), low MgO content (0.93 to 3.52 wt.%), P_2O_5 (avg. 0.12 wt.%), TiO_2 (avg. 0.32 wt.%), and LOI (avg. 2.50 wt.%) (SDT III). These geochemical features indicate that the paternal magma is andesitic to basaltic nature (Tahirkheli et al., 2012). According to an AFM (Na_2O + K_2O- FeOT - MgO) diagram, the analyzed diorites fall within the calc-alkaline category (Figure 9a). On the diagram by (Frost and McCammon, 2008), the granitoids from Danyore Valley appear to have magnesian characteristics (Figure 9b). Based on the A/CNK vs A/NK plot, the studied diorites are metaluminous in characteristics, except for one sample that was plotted on peraluminous (Figure 9c). The analyzed diorites exhibit significant similarities in major oxide composition to those found in the Kohistan batholith (Petterson et al., 1985).

The investigated dioritic rock displays varying concentrations of Ni (1.73 ppm), Cr (10 ppm), and Co (4.40 ppm). High field strength elements (HFSEs), including Nb (7.93 ppm), U (4.82 ppm), Ta (0.31 ppm), Hf (3.83 ppm), and Th (17.32 ppm), exhibit depleted levels, with Zr being the exception, showing a slightly more comprehensive range at 146 ppm (SDT III). Conversely, the significant ion lithophile elements (LILEs) exhibit notable concentrations, with Ba at 260 ppm, Rb at 38.83 ppm, and Sr at 617 ppm. The spider-normalized diagrams of Danyore Valley diorites (Boynton, 1984; McDonough and Sun, 1995) possess fragmented trace element structures with lower HREE and elevated LREE element concentrations.

Preprints.org (www.preprints.org) | NOT PEER-REVIEWED | Posted: 13 May 2024 doi:10.20944/preprints202405.0851.v1

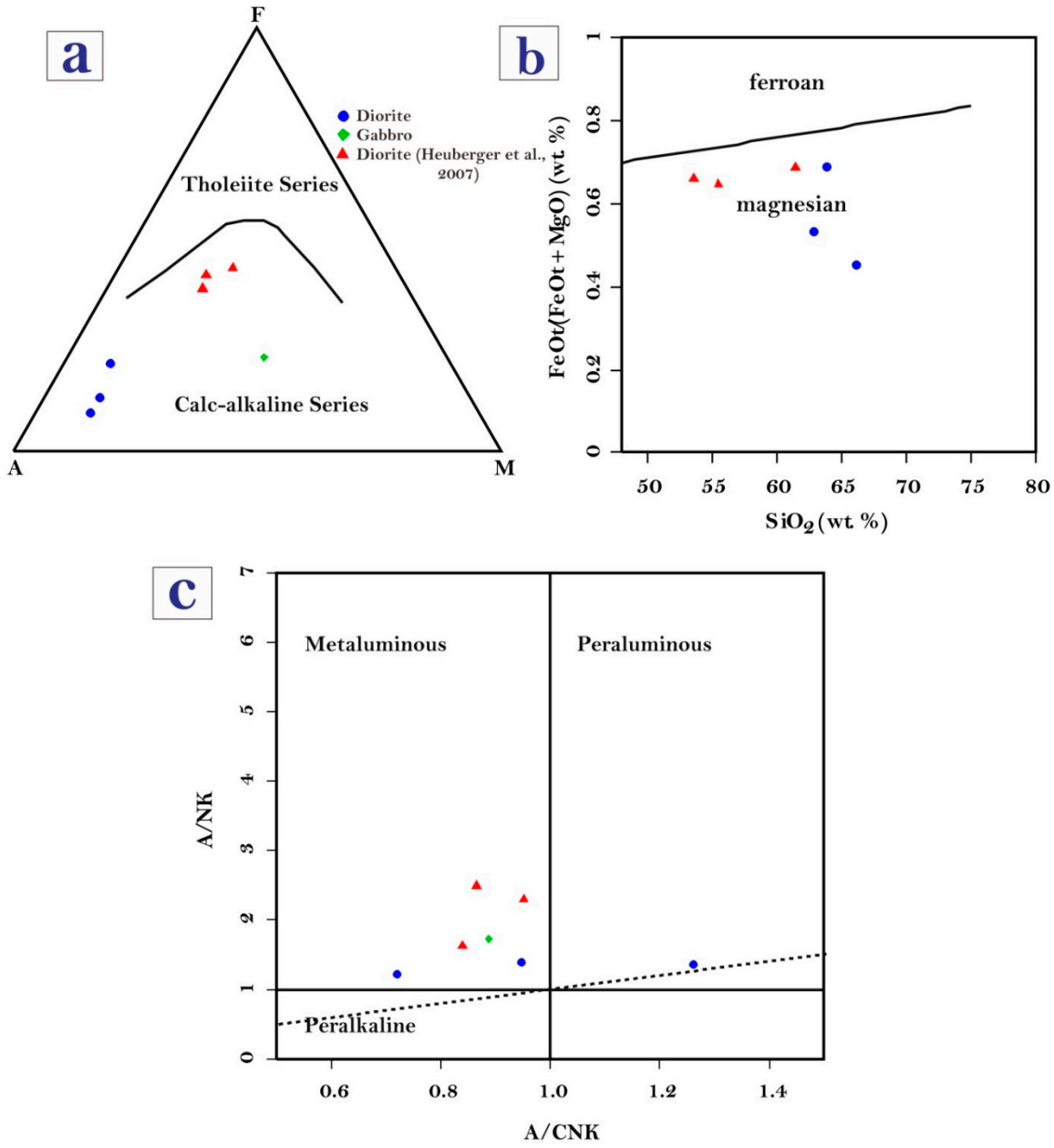

Figure 9. Magma type discrimination plots of hosting rocks of Danyore Valley copper-gold prospect, Northern Pakistan: (a) AFM diagram (Irvine and Baragar, 1971) showing a tholeiitic to calc-alkaline trend; (b) $FeO^T/(FeO^T + MgO)$ vs. SiO_2 diagram (Frost et al., 2001); (c) A/CNK [molar ratio $Al_2O_3/(CaO + Na_2O + K_2O)$] vs. A/NK [molar ratio $Al_2O_3/(Na_2O + K_2O)$] diagram after (Shand, 1942).

4.3.2. Gabbro

The studied gabbro rock expresses a limited extent of SiO_2 (43.22 wt.%), low MgO (8.97 wt.%), Na_2O (2.23 wt.%), and K_2O (6.08 wt.%). Similarly, low TiO_2 (1.11 wt.%), P_2O_5 (0.20 wt.%), and a moderate range of Al_2O_3 (17.68 wt.%), CaO (5.32 wt.%), and Fe_2O_3 (5.47 wt.%) (SDT III). The LOI value of gabbro rock is 4.31 wt.%. According to the classification graph of alkali-total iron magnesium (AFM) (Irvine and Baragar, 1971), the gabbro rocks predominantly belong to the calc-alkaline category (Figure 9a). Based on the diagram A/CNK vs A/NK (Shand, 1942), the studied gabbros are metaluminous (Figure 9b).

The studied gabbro rock is illustrated by varying concentrations of Co (12.6 ppm), Cr (470 ppm), and Ni (132 ppm). Concentrations of high field strength elements (HFSE) include Ta (0.60 ppm), Nb (8.8 ppm), U (1.61 ppm), Hf (2.4 ppm), Th (1.71 ppm), and Zr (110 ppm). Conversely, large ion lithophile elements (LILEs) have substantial concentrations (Sr = 577 ppm, Ba = 300 ppm, and Rb =

Preprints.org (www.preprints.org) | NOT PEER-REVIEWED | Posted: 13 May 2024 doi:10.20944/preprints202405.0851.v1

144 ppm). The normalized primitive mantle and REE chondrite behaviors are distinguished by the enrichment of LILE-LREE compared to the decreased HFSE and HREE (Figure 10a,b). The normalized patterns show significant positive deviations in Rb, Pb, and P (Figure 10a). The rare earth element (REE) distribution in the gabbro samples demonstrates a marginal rightward trend, and there are noticeable dips in Eu with weak negative anomaly (Figure 10b).

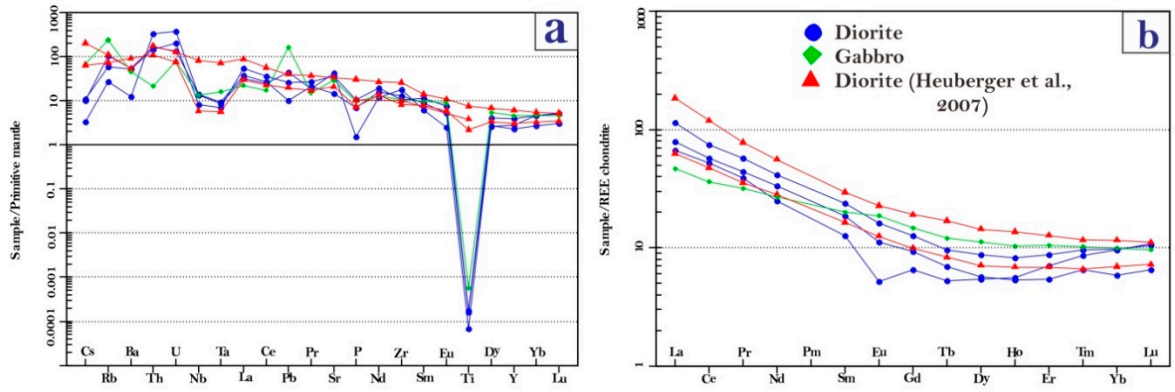

Figure 10. (a) Primitive mantle-normalized spider diagram (McDonough and Sun, 1995) and (b) chondrite-normalized REE (Boynton, 1984) for hosting rocks of Danyore Valley copper-gold prospect, Northern Pakistan.

4.4. Mineralization Style and Sulfide Chemistry

In the Danyore Valley area, mineralization predominantly occurs in association with sulfide-rich quartz veins and extensive alteration assemblages (Figure 11a–c). The orientation of the veins is predominantly NW, although some veins exhibit NE trends. The outcrops of Cu-Au mineralization are visible at over 35 different locations (Figure 11a,d,g,j). They appear as either discontinuous horizontal to vertical quartz veins, sulfide-rich quartz veins, or less commonly massive ore. The mineralized masses have a dimensions ranging from 1 to 5.5 meters, with inconsistent lengths ranging from 14 to over 900 meters.

A significant portion of quartz veins exhibits notable abundance in primary sulfide minerals, including chalcopyrite and pyrite grains, which can be clearly observed in the field and collected hand specimens (Figure 11b). Microscopically, chalcopyrite, pyrite (Figure 11f–i), and bornite are the major components of the quartz veins rich in sulfides (Figure 11l). The most prevalent sulfide mineral is chalcopyrite, which is preceded by pyrite, sphalerite, and bornite in decreasing abundance in the Danyore Valley area. A summary of the paragenetic correlations associated with ore minerals and alteration assemblages is given in Figure 12. The EPMA results for the selected minerals (i.e., chalcopyrite, pyrite, and bornite) are presented in SDT IV.

Chalcopyrite is the predominant mineral found in sulfide-rich quartz veins. It is typically correlated with sphalerite, bornite, and pyrite, the latter usually forming a ring around the major sulfides (Figure 11c,f,l). Chalcopyrite predominantly interacts with silicate minerals and coarse-textured euhedral quartz. It can be distinguished by euhedral or subhedral and irregularly distributed grains/textures. Chalcopyrite commonly forms continuous bands that vary from 500 μm to 5 mm thick. Furthermore, it frequently occurs with sphalerite as chalcopyrite illness. It is primarily interlocked with sphalerite, covellite and bornite, it is often altered by the secondary minerals bornite and covellite across its outer edges. The S and Fe Average concentrations in the chalcopyrite are 33.54 to 53.96 and 29.99 to 46.97 (avg 37.86 & 33.30 wt%), the Cu and Au concentrations are 0.008 to 35.62 wt% and 30 to 1230 ppm (avg 34.73 wt.% & 324 ppm) (SDT IV). The chalcopyrite mineral has also been analyzed for As, Se, Si, Pb, Ag, Zn, Ni, Mn, Te, Sb, Te, and Cd. Average trace element Concentration of Se 264, As 196, Ag 134, and Te 294 ppm, Pb 0.037, Zn 0.035, Ni 0.013, Mn 0.010, Sb 0.012, and Cd 0.023, while Si showed concentration below the detection limit.

Preprints.org (www.preprints.org) | NOT PEER-REVIEWED | Posted: 13 May 2024 doi:10.20944/preprints202405.0851.v1

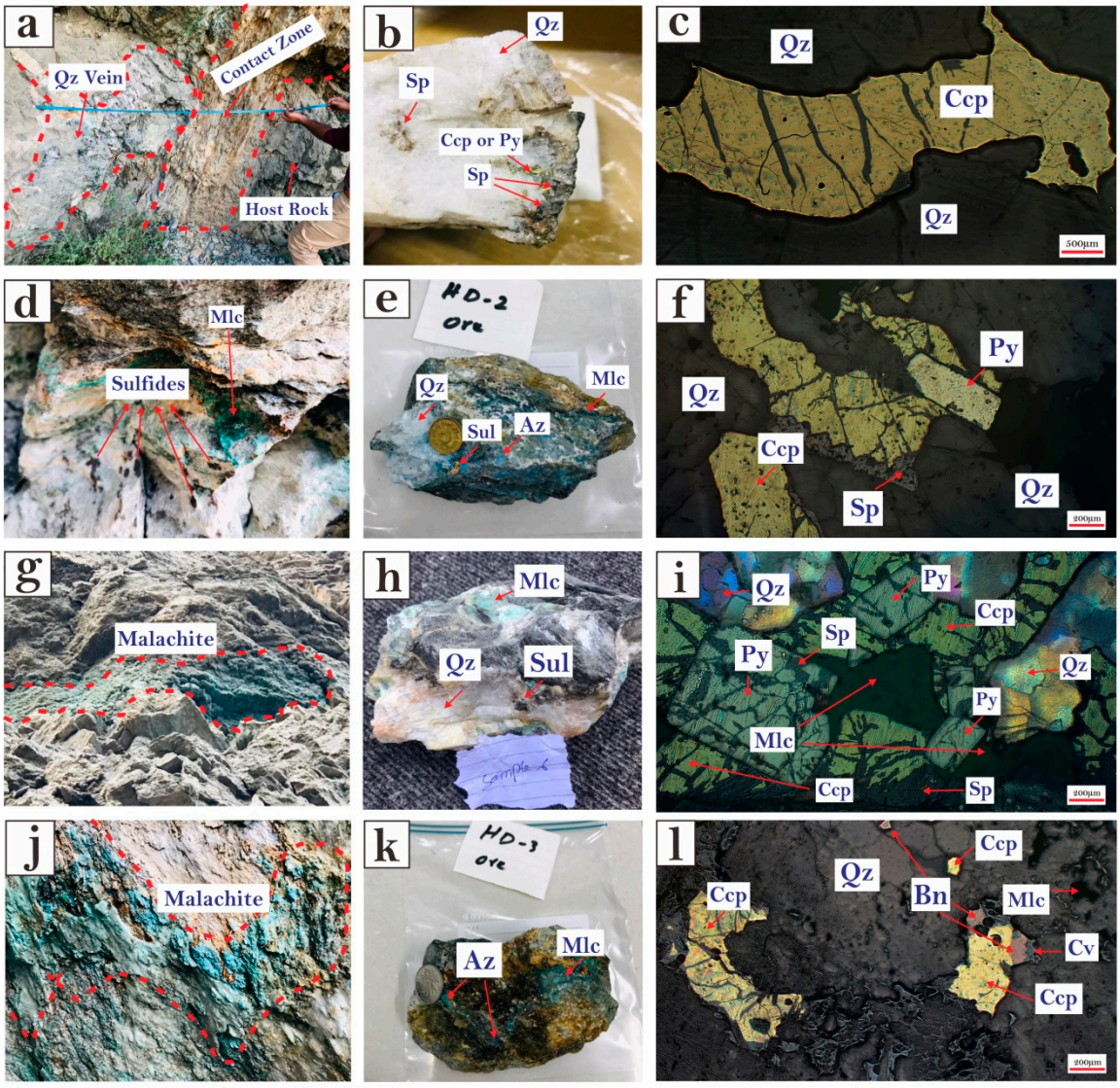

Figure 11. Field photographs of mineralization style, ore hand specimens and microphotographs of studied minerals: (a) outcrop of sulfide bearing quartz vein at left side, host rock diorite at right side, highlited brown colour is the contact zone which is highly altered and deformed, displaying the features of shearing; (b) ore hand specimen from quartz vein showing chalcopyrite, pyrite, and sphelarite; (c) microphotograph shows large 500 µm euhedral chalcopyrite crystal, PPL; (d) field photograph showing the malachite, black colour dots indicating (sulfides and iron oxides); (e) representive ore sample showing malachite, azurite, and sulfides (Ccp and Py) with gangue quartz; (f) microphotograph showing subhedral chalcopyrite grains with cubic pyrite and sphelarite at the boundary of chalcopyrite and gangue mineral quartz, PPL; (g) outcrop photographs from field showing large scale exposure (up to 1-1.5 m in length) of secondary copper mineralization, including malachite, azurite, and native copper; (h) ore sample from sulfide bearing quartz vein displays malachite and sulfides (Ccp and Py); (i) photomicrograpghs showing large 200 µm cubic pyrite grain interlocking with subhedral chalcopyrite, sphalerite replaced or reformed at the boundry of pyrite and chalcopyrite, secondary mineralized malachite at the center of chalcopyrite and pyrite, XPL; (j and k) copper ore showing iron oxidation surrrounding malachite and azurite secondary carbonate minerals; (l) microphotograph showin euhedral chalcopyrite grains, bornite at the boundry of chalcopyrite, bornite is converted to covellite, malachite as a secondary mineralized mineral, PPL. Abbreviations: Qz (Quartz), Py (Pyrite), Ccp (Chalcopyrite), Sp (Sphalerite), Bn (Bornite), Cv (Covellite), Mlc (Malachite), Az (Azurite), Sul (Sulfides), XPL (Crossed polarized light), PPL (Plain polarized light).

Preprints.org (www.preprints.org) | NOT PEER-REVIEWED | Posted: 13 May 2024 doi:10.20944/preprints202405.0851.v1

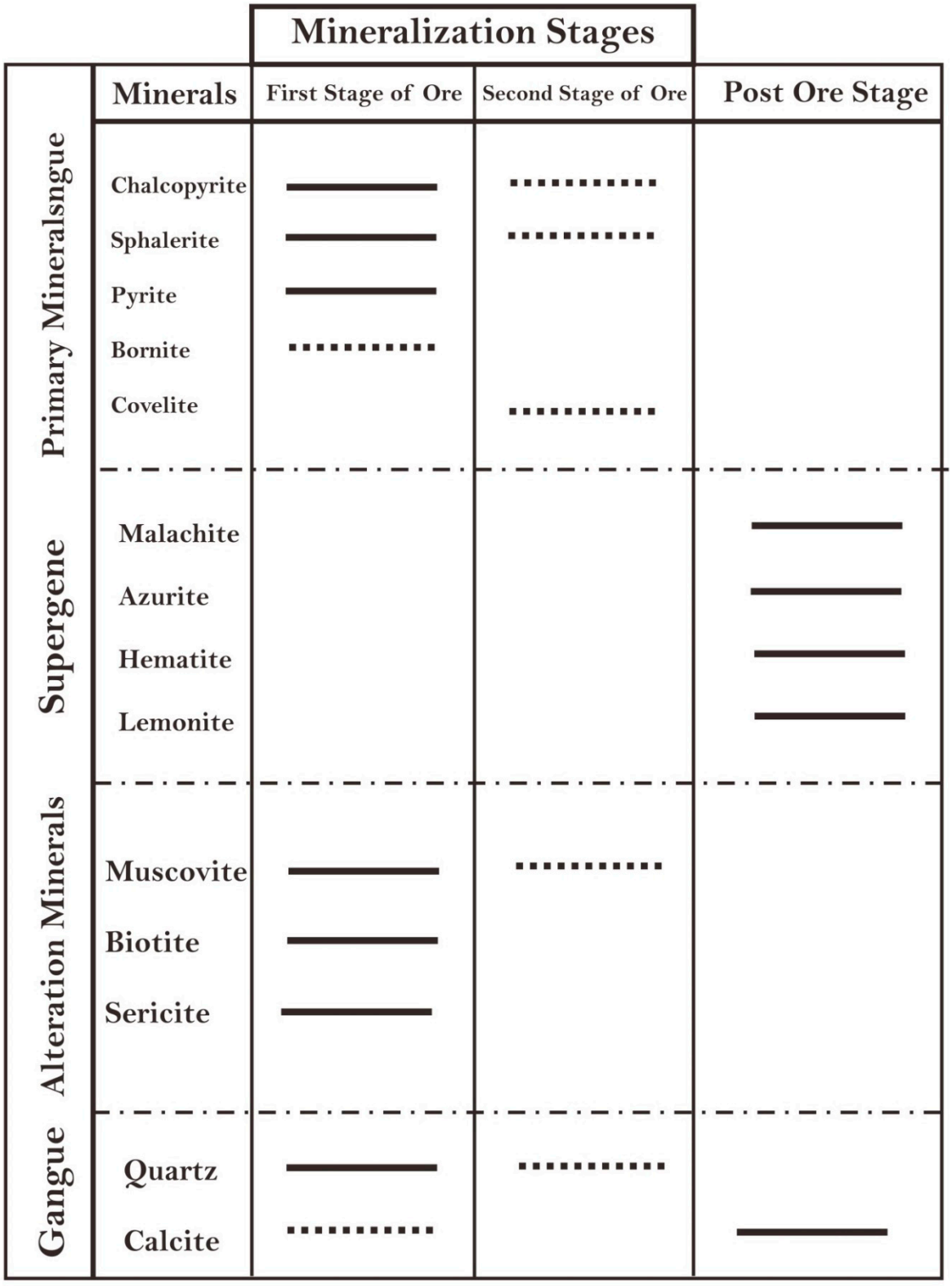

Figure 12. Mineral assemblages and paragenetic sequence of sulfide-bearing quartz veins in Danyore Valley prospect, Northern Pakistan. Higher abundances are represented by thick bars, while lower abundances are indicated by thin and dashed lines.

Pyrite is the most frequently occurring mineral encountered in quartz veins rich in sulfides, pyrite outgrows sphalerite and is being witnessed forming massive euhedral to subhedral cubic grains and rhomboidal crystals along to cracks (Figure 11d–f). The pyrite crystals have a grain size ranging from 50 μm to 6 mm. It mostly appears with euhedral to subhedral crystals of quartz and

Preprints.org (www.preprints.org) | NOT PEER-REVIEWED | Posted: 13 May 2024 doi:10.20944/preprints202405.0851.v1

infrequently occurs with other sulfides. Most of the pyrite grains show similar contents of S 52.32 to 53.96 (avg. 53.17 wt.%) and Fe 46.14 to 46.93 (avg. 46.5 wt.%) in comparison with their reference concentrations (Farhan et al., 2023) (S = 53.45 wt.% and Fe = 46.55 wt.%) (SDT IV). Trace elements average contents above the detection limit, such as Se 106, As 138, Au 250, Ag 25, and Te 444 ppm, whereas Ni 0.014, Sb 0.005, Si, Mn 0.012, Zn 0.023, and Cd 0.028 wt%. Cu, Si, and Pb are undetectable in all investigated grains (SDT IV).

In large chalcopyrite grains, boronite has been found sporadically and as oriented mineral exsolution flakes, mainly found in association with quartz veins rich in copper (Figure 11k,l). Bornite crystals have a grain size ranging from 10 μm to 2 mm. Chemically, bornite is nearly equimolar, the Cu, S, and Fe concentrations (wt%) are 58.54 to 63.81, 24.99 to 28.19, and 11.21 to 12.68 (Avg. 62.44, 25.97, and 11.70) (SDT IV). Trace elements concentrations above the detection limit are As 330, Se 473, Au 220, Ag 683, and Te 217 ppm, Zn 0.036, Mn 0.007, and Cd 0.013, while Si, Pb, Sb and Ni showed concentrations below the detection limit.

The mineralized quartz veins are located primarily within the altered diorites and gabbros. The boundary between the mineralized region and the adjacent country rock is distinct and accurate, sometimes showing a gradual transition in some places within the study area.

The supergene enrichment assemblage is extensive and is characterized by the presence of large exposure (up to 1-1.5 meters in length) of carbonate copper minerals. They comprise azurite, malachite, chrysocolla, and native copper (Figure 11g-j). These areas are surrounded by high iron-rich gossan materials, consisting of limonite, hematite, and goethite minerals (Figure 11k). It is most likely that post-depositional activities significantly participated in the liberation, transportation, and redeposition of Cu that had probably been extracted from a hidden ore body or pre-existing country rocks. The primary gangue materials include calcite, biotite, and quartz, along with a small percentage of muscovite and feldspar.

4.5. Alteration Assemblages

Hydrothermal alterations appear close to the sheared zones and along the boundary among the wall rock and quartz veins containing sulfides. (Figures 4 and 11). The sulfide-quartz veins are locally surrounding by three pertinent hydrothermal alterations: propylitic, phyllic, and carbonatization assemblages. Among them, propylitic and phyllic alteration are specifically essential for the mineralization process. These alterations patterns typically appear within a range of about 1 to 3 meters away from mineralized masses, displaying a vein-like distribution, particularly evident in close proximity to the veins. The most frequently encountered hydrothermal gangue minerals are quartz and calcite.

4.5.1. Phyllic Alteration

This type of alteration appears in the outer part, at the interface with the host rock (diorite and gabbro). It is identified by the assemblage of sericite + quartz + pyrite. Sulfide-bearing quartz vein is occasionally covered and surrounded by a small parallel muscovite layer (Figure 13a). The microscopic studies reveal that the feldspars of country rocks are typically replaced by sericite and clay minerals (Figure 13b). Sericitization assemblage is composed of subhedral to anhedral sericite with a fine to medium grain size and microcrystalline quartz (Figure 13a). The presence of sericite in fine-grained quartz would have been attributed to silicification, which is the release of silica during plagioclase sericitization. Therefore, sericite and quartz are frequently formed together. (Figure 13a–c).

Preprints.org (www.preprints.org) | NOT PEER-REVIEWED | Posted: 13 May 2024 doi:10.20944/preprints202405.0851.v1

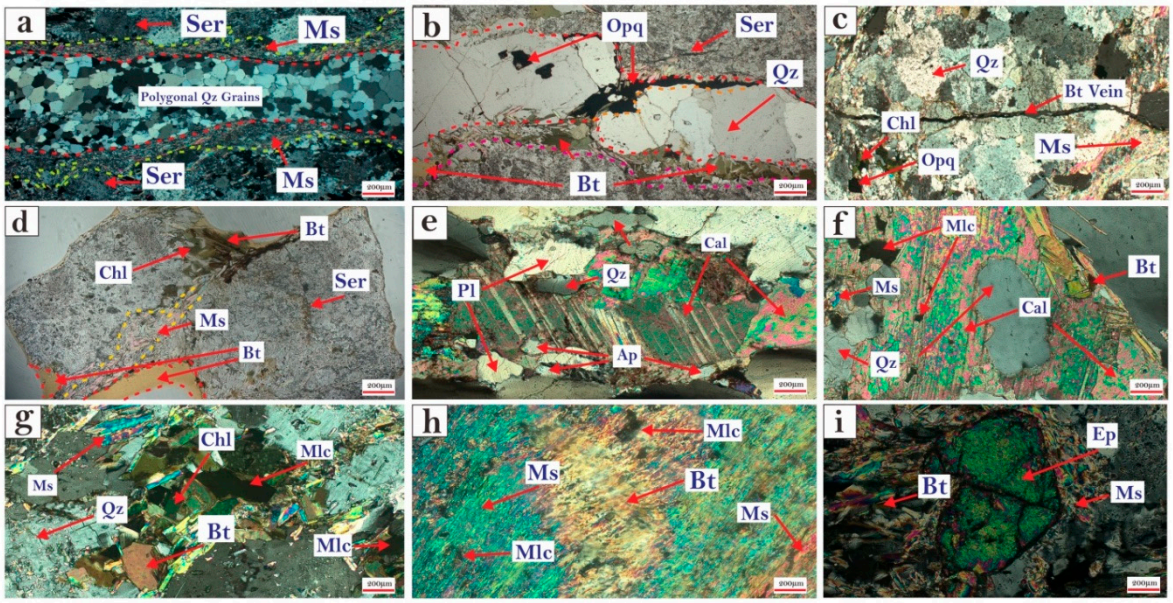

Figure 13. Representative microphotographs (cross-polarized light, XPL and Plain polarized light, PPL) of alteration types: (a) polygonal quartz grain vein is surrounded by musovites at both sides, plagioclase is altered to sericite, PPL; (b) Quartz vein with large euhedral grains, biotite at the boundry of quartz vein, sericitizaton alteration at wall rock contact, opaque minerals at the center of quartz veins (sulfides or ironoxides), PPL; (c) moderately altered quartz with altered muscovite, biotite completely altered to chlorite, opaque minerals (sulfides or iron oxides), XPL; (d) plagioclase completely altered to sericite, biotite altered into cholrite, PPL; highly altered calcite at the right side with slightly altered plagioclase and quartz, apatite as accessary mineral, XPL; (f) large euhedral quartz grain at the center of altered carbonate mineral (calcite), altered muscovite and secondary mineralized malachite, XPL; (g) biotite completely altered into chlorite with altered muscovite, quartz and malachite, XPL; (h) highly altered biotite at center with highly altered muscovite, malachite is indiccating secondary mineralization; (i) large epidote grain with altered biotite and muscovite. Abbreviations: Qz (Quartz), Bt (Biotite), Pl (Plagioclase), Ap (Apatite), Ms (Muscovite), Chl (Chlorite), Ep (Epidote), Cal (Calcite), Opq (Opaque), Mlc (Malachite), Ser (Sericite), XPL (Crossed polarized light), PPL (Plain polarized light).

4.5.2. Propylitic Alteration

This kind of mineralogical aggregate consists of biotite, chlorite, epidote, muscovite, and pyrite with a minor amount of carbonate minerals (e.g., calcite) and bornite. Host rocks close to the mineralized area are relatively altered and contain some disseminated and sulfide stringers, which possess geometric connectivity to quartz veins. All grains of sulfide are euhedral without post-formation changes. Microscopic observation indicates that the biotites were replaced by chlorite and epidote (Figure 13g). Chlorite is mainly recognized as a predominant mineralogical phase commonly resulting from the alteration of hornblende and biotite.

In some places along the Danyore Valley area, the propylitic alteration is generally appeared as unevenly distributed to the pre-ore alteration minerals and sulfide-rich veins (Figure 13i). More specifically, a substantial quantity of quartz, biotite, and epidote assemblages dominate the epidotization alteration. These minerals represent sequential patterns or aligning appearances in any scenario and they have subhedral to anhedral fine grains. The altered felsic granitoids are primarily crosscut by the later phase of calcite veins. (Figure 13e).

4.5.3. Carbonatization Alteration

Carbonatization is occasionally observed away from the mineralized area. The carbonate-quartz region is primarily constituted of sterile quartz and calcite formed in the later stages. Most calcite grains are slightly altered and associated with a minor amount of apatite mineral (Figure 13e). Many

Preprints.org (www.preprints.org) | NOT PEER-REVIEWED | Posted: 13 May 2024 doi:10.20944/preprints202405.0851.v1

euhedral quartz crystals indicate that the growth of hydrothermal ore-forming fluids lessened and was subsequently terminated.

5. Discussion

5.1. Age of Gabbro-Diorite Intrusion from Danyore Valley Area

In general, earlier workers (Auden, 1935; Burg et al., 2006; Griesbach, 1893; McMahon, 1884; Treloar et al., 1989; Wadia, 1928) attempted to determine the ages of the diorites and gabbros from Kohistan Batholith on the basis of structural behaviors, xenolith composition, petrological Imprints, and field correlations. However, the need for accurate geochronology indicates significant uncertainties regarding the timing of the emplacement of these granitoid bodies. (Treloar et al., 1989) initiated the Ar-Ar dating on the Matum Das Pluton (81 Ma) and Naz Bar Pluton (granite 84 Ma, diorite 82 Ma, and granodiorite 80 Ma) in the Kohistan Batholith. Furthermore, according to the tectonic map of the north of Pakistan, neighboring areas of northern Ladakh, and western Tibet by Zanchi et al. (2011), the age of the calc-alkaline gabbro-diorite units of the Kohistan Batholith is 110 to 90 Ma (Rb-Sr dating). The Kohistan batholith's age of granodiorite and granite rocks is 85 to 40 Ma, by the K-Ar and Rb/Sr dating methods (Treloar et al., 1989). Diorites from Shunji pluton and Pingal pluton (Kohistan Batholith) located approximately 101 km from my study area given an age of 64.5 ± 0.5 Ma and 41.0 ± 0.5 Ma based on the U-Pb zircon dating technique (Khan et al., 2009).

Five intrusive rock samples collected from the Danyore Valley region (Kohistan Batholith) were dated utilizing the LA-ICPMS zircon U-Pb age dating technique. (SDT I and Figures 5–7). The U-Pb isotopic analysis of studied zircons from the diorite specimens provided a concordia age of 111.60 ± 0.90 Ma (MSWD = 0.41) to 112.18 ± 0.74 Ma (MSWD = 0.17) (Figures 5 and 6). Correspondingly, the gabbro rock sample (SD-9) displayed a concordia age of 110.21 ± 0.99 Ma (MSWD = 0.98). The crystallization age of studied gabbro-diorite units from the Danyore Valley area is largely in agreement with those reported from the Gawuch Village area (Kohistan batholith), situated approximately 227 km northwest of Gilgit. The gabbro and diorite rocks from this area give an age range between 106.7 and 107.2 Ma according to the U-Pb age dating system (Heuberger et al., 2007).

5.2. Tectonic Setting of Gabbro-Diorite Intrusion

There is a debate in the literature about the tectonic context of the Kohistan Batholith, ranging from a continental rift environment (Petterson, 2010) to an island arc setting (Petterson et al., 1991). Besides, some researchers (Treloar et al., 1989; Treloar et al., 1996) contend that the batholith is an instance of magmatism associated with subduction. In contrast, others (Petterson et al., 1985; Searle et al., 1987) have argued that it originates from magmatism originating from continent collisions. However, the Kohistan Batholith is probably the product of the subduction and collision of tectonic plates (Searle et al., 1999). Samples taken from the Kohistan Batholith showed that it represented a continental arc arising from the downward movement of the Indian plate below the Eurasian plate (Searle et al., 1987).

Generally, zircons from continental crust and ocean crust are distinguished using the proposed discrimination diagram of (Grimes et al., 2007). The U/Yb vs Hf, tectonic setting classification diagram predominantly illustrates that the zircons from the researched area fall within the continental zircon domain (Figure 14c), revealing the continental nature of these rocks. On the other hand, there is a dispute regarding which sources originated massive amounts of post-collisional calc-alkaline, predominantly mafic magmas, from which the analyzed zircons formed (Petterson et al., 1991). Several theories propose that these magmas emerged from partially melting either subducted oceanic crust or from the anatexis of earlier island arc crust (Ashraf, 1999). The Sm versus Gd/Yb discrimination plot is usually used to identify the origin of zircon from different tectonic settings based on its trace element content (Grimes et al., 2007). It displays that all analyzed zircons from the Danyore Valley copper prospect have been mainly positioned outside the fields of an arc and a MORB environment, suggesting the continental origin (Figure 14d). Considering the likely association of the

Preprints.org (www.preprints.org) | NOT PEER-REVIEWED | Posted: 13 May 2024 doi:10.20944/preprints202405.0851.v1

study area's diorites with the Gawuch formation in Chitral, which has an age of 110-112 Ma, proposed that these rocks originated in a continental margin tectonic environment (Heuberger et al., 2007).

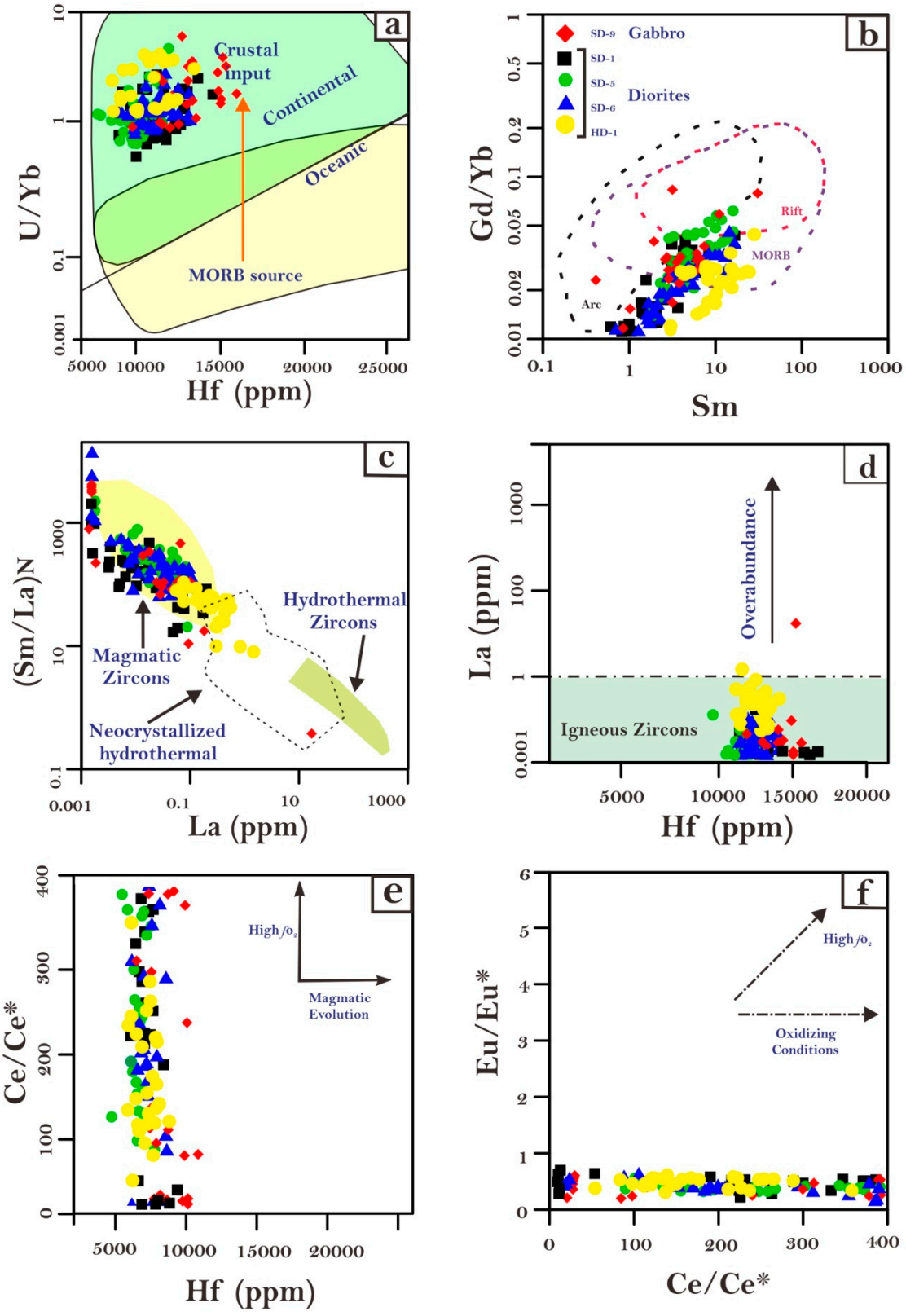

Figure 14. Zircon trace element discrimination diagrams of the gabbro and diorite hosting rocks: (a) $(Sm/La)_N$ vs. La diagram: data for hydrothermally recrystallized zircons are from (Kirkland et al., 2015); magmatic and hydrothermal zircon values are from (Grimes et al., 2009) and (Hoskin, 2005);

Preprints.org (www.preprints.org) | NOT PEER-REVIEWED | Posted: 13 May 2024 doi:10.20944/preprints202405.0851.v1

(b) La_N vs. Hf plot, data for igneous zircon fields are from (Hoskin et al., 2003); (c) U/Yb vs. Hf diagram, continental and oceanic crust data are from (Grimes et al., 2007); (d) Gd/Yb vs. Sm tectonic setting plot, dashed regions indicate the range of zircon geochemistry (after (Carley et al., 2014); (f) Hf vs Ce/Ce*; (e) Ce/Ce* vs. Eu/Eu* diagram.

Identifying the genetic type of granitoids from whole rock geochemistry is crucial for comprehending the evolution, magma sources, and tectonic settings (Pearce et al., 1984; Sylvester, 1998). According to Zr against 10,000 Ga/Al and Ce versus 10,000 Ga/Al discrimination graph (Figure 15a), granitoids from the Danyore Valley prospect fall within S- and I-type granites.

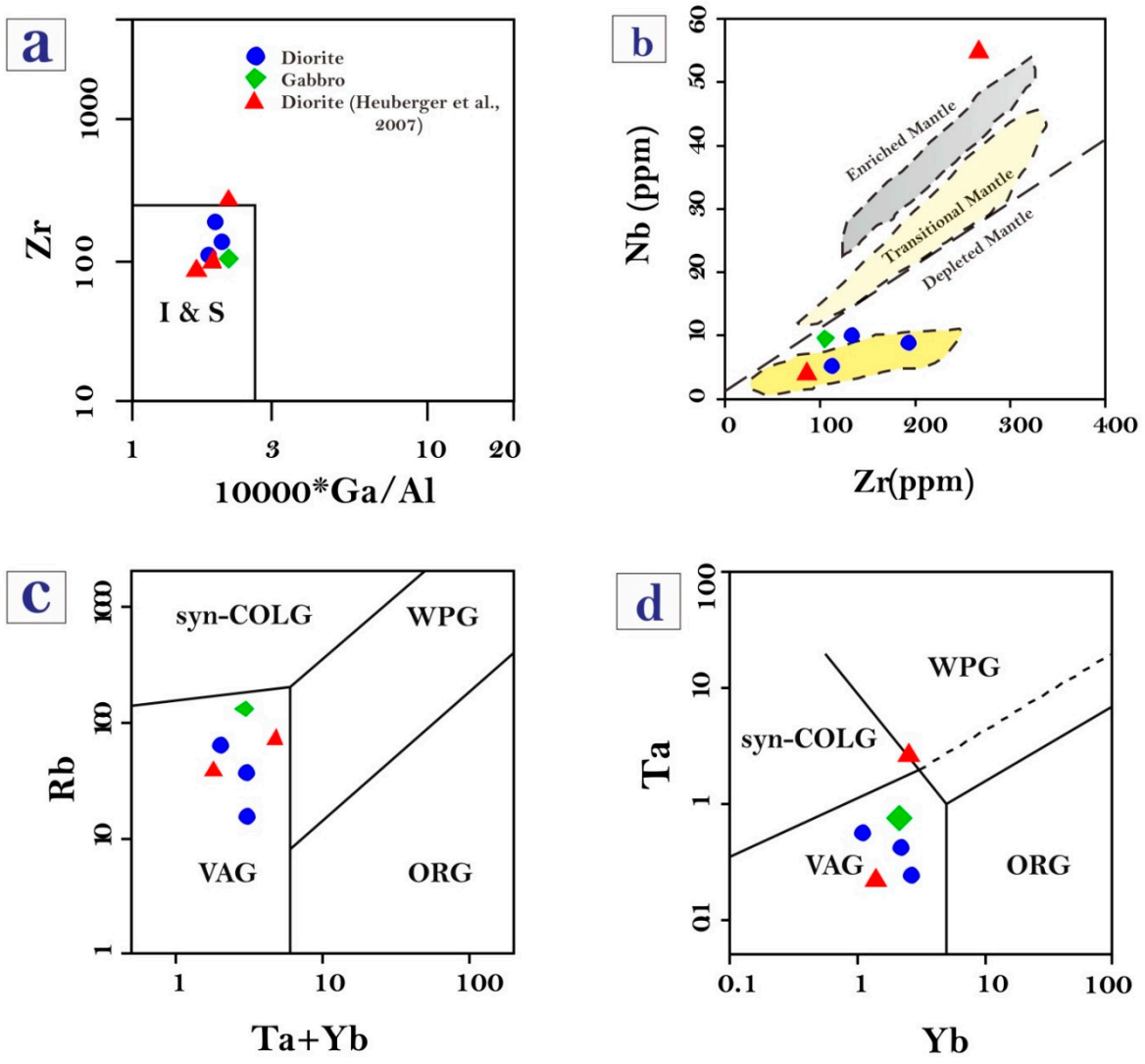

Figure 15. Tectonic discrimination diagrams of the Danyore Valley area, Northern Pakistan: (a) Zr vs. 10,000*Ga/Al (Pearce et al., 1984), (b) Ce vs. 10,000*Ga/Al (Pearce et al., 1984), (c-d) Ta+Yb vs Rb and Yb vs Ta diagrams (Pearce et al., 1984), (e) Zr - Nb (ppm) diagram (Geng et al., 2011).

On the tectonic discriminant diagram, the diorites and gabbro from the study area primarily lie on the "volcanic arc granite (VAG)" field, as observed in the Ta+Yb against Rb plot (Figure 15c). Additionally, based on the Yb vs Ta tectonic graph (Pearce et al., 1984), the analyzed granitoid rocks are plotted within the volcanic arc area, with one specimen identified in the syn-collisional granite region (Figure 15d). Spider graphs of the primitive mantle to normalized compositions suggest that gabbros and diorites exhibit depletion in High Field Strength Elements (HFSE), including Eu, Li, Ti,

Preprints.org (www.preprints.org) | NOT PEER-REVIEWED | Posted: 13 May 2024 doi:10.20944/preprints202405.0851.v1

and P, along with enhancement in Large Ion Lithophile Elements (LILE), in particular U and Ba (Figure 10a,b).

The Zr-Nb (ppm) ratio has the potential to indicate mantle depletion or enrichment, as suggested by (Geng et al., 2011). Analysis results from the Danyore Valley diorites and gabbros position within the depleted mantle field (Figure 15b), this depletion pattern suggests similarities to certain island arc basalts. The investigated gabbro and diorite specimens are most likely products of a partially melted or depleting asthenospheric mantle that has undergone metasomatism due to subduction-related fluids. Furthermore, the tectonic setting of the Danyore Valley granitoids is mainly consistent with the geodynamic environment of gabbro-diorite of the Kohistan Batholith, which primarily generated in a subduction-related environment (Jagoutz et al., 2009; Petterson et al., 1985).

To sum up, the host rock units of the Danyore Valley copper prospect predominantly plot within the continental arc field and have calc-alkaline signature with arc-like geochemical features.

5.3. Petrogenesis of Danyore Valley Intrusion

The granitoids from the Danyore Valley area of Kohistan Batholith are identified as calc-alkaline, I-type granitoids, comprising diorites and gabbro. The diminution of high field-strength elements (HFSE): Ta and Nb Figure 10a) is a typical geochemical feature of arc magma generated in the subduction zone (McCulloch et al., 1991), This observation further supports the integral supra-subduction area classification of the Kohistan Batholith, as initially proposed by (Tahirkheli, 1979). Studied diorites exhibit high SiO_2, medium to high K calc-alkaline, metaluminous properties, and possess relatively elevated sodium contents (Na_2O = 2.23–6.61 wt.%, with a mean concentration of 6.14 wt.%). These features suggest that the granitoids of Danyore Valley are typically identical to I-type granite characteristics (Chappell et al., 1992).

The high aluminum with andesitic magma nature is evident in the examined diorites. This type of magma is commonly generated in subduction-related environments, especially at continental edges (Wilson, 1989). Gabbroic rocks may originate from either Arid or moist basaltic magma during a mechanism of fractionated crystallization (Gaetani et al., 1998). The samples exhibit generally comparable trends on normalized-primitive mantle trace element graphs (Figure 10a,b), demonstrating large-ion lithophile elements (LILE) enrichment and notable reductions in Ti, Nb and Ta. These characteristics are typical of magmas associated with arcs (Briqueu et al., 1984; Brown et al., 1984; Gill et al., 1981). Gabbros and diorites show comparable compositions regarding Rare Earth Elements (REE) and trace elements. They also demonstrate comparable chondrite normalized REE distribution trends, with only slight variations in total amount and Eu/Eu* ratios. These similarities suggest a common source for both rock types and imply an evolutionary familial relation.

The studied rock samples display a calc-alkaline pattern, as illustrated in (Figure 9a) and show variations in SiO_2 ranging from 45% to 66%. Also, there is a lesser content in K_2O, MgO, and TiO_2, and an increase in Al_2O_3, CaO, FeO, and Na_2O suggesting a fractionation trend. Gabbros and diorites demonstrate high concentrations in Rb, Ba, U, and LREE relevant to K, Zr, Ti, Y, and HREE, indicating an arc-like geochemical signature. These trends in geochemistry indicates that the primary magma source of the studied plutonic rocks from the Danyore Valley area is generated from the fractional melting of depleted upper mantle source, which is enriched in LREE elements, followed by a fractionation crystallization process during their ascent through the mantle/crust and final emplacement. It is highly harmonic with the proposed formation model of granitoids from Kohistan Batholith by Petterson et al. (1985).

Detectable amounts of high-field strength element (HFSE) were found in all of the analyzed zircons. Ti, Nb, and Ta contents are less than 75 ppm, 62 ppm, and 3 ppm, respectively, suggesting a typically average abundance of magmatic zircons (Faisal et al., 2020; Hoskin et al., 2003). Conversely, magmatic and hydrothermal zircons could be distinguished by using binary diagrams of Hoskin (2005); Kirkland et al. (2015). Based on the data shown in the La against $(Sm/La)_N$ graphs (Figure 14a), the majority of the investigated specimens from the Danyore Valley area had low La and high $(Sm/La)_N$, which is the characteristic of unchanged magmatic zircons (Grimes et al., 2009; Hoskin, 2005). Some grains plotted between the neo-crystallized hydrothermal zone and magmatic field,

Preprints.org (www.preprints.org) | NOT PEER-REVIEWED | Posted: 13 May 2024 doi:10.20944/preprints202405.0851.v1

indicating that these grains may have undergone subsequently hydrothermal alteration and recrystallization after the gabbro-diorite emplacement.

La (N) versus Hf (Figure 14b) plot illustrates the excessive of LREE in the dated zircons. LREE (La and Pr) typically have sub-ppm to ppm-range absolute overages in igneous zircon, However, Ce abundances may reach up to about 50 ppm, which is considerably more compatible with magmatic zircons (Schaltegger et al., 2009). All examined zircons from the Danyore Valley prospect are plotted within the normal range of igneous zircon abundance in the Hf vs. La discrimination diagram (Figure 14b), confirming the magmatic origin for these zircon grains.

Monitoring changes in oxidation state during magma differentiation can be achieved by studying the trace elements of zircon. It is widely accepted that the impact of mineral crystallization on the abundances of Ce and Eu depletion is dependent on the state of oxidation (Hoskin et al., 2003; Trail et al., 2012; Xia et al., 2011). Therefore, the oxygen fugacity of the magma is often associated with the oxidation phase of rocks. In their comparably low LREE patterns, the zircons displayed substantial positive Ce anomalies, while Eu anomalies are mainly negative. Discremination diagram of Hf vs. Ce/Ce* (Figure 14e) shows that most zircons fall within the restricted spectrum of oxygen volatility with increasing magma growth (elevated Hf), suggesting that relatively reduced settings (low oxygen fugacity) which were employed for the initial crystallization.

For identifying the oxidation state at the magma formation, the Ce/Ce* vs Eu/Eu* (Figure 14f) diagram is an invaluable resource (Trail et al., 2012). Variations in the anomalies of Ce and Au may be understood as indications of the physiochemical crystallization process of zircon. Zircon possesses distinctive properties in its Rare Earth Element (REE) pattern. (Ballard et al., 2002; Barth and Wooden, 2010; Burnham and Berry, 2012; Claiborne et al., 2010; Li et al., 2014; Pettke et al., 2005; Trail et al., 2012; Trail et al., 2011). The recent application of Ce and Eu contents in zircons for oxybarometry is due to their sensitivity to magmatic oxidation states, driven by their ionic states. The degree of negative Eu anomaly can be influenced by the redox condition during the formation minerals from a hydrothermal fluid or molten substance. (Hoskin et al., 2003; Trail et al., 2012; Xia et al., 2011). Most zircons from the units under investigation exhibited an inverse relationship tendency when approaching to the oxidation phases. The Eu-anomaly noticed in this research is considered to originated from the Eu-deficient melt subjected to reduced environments due to the unfavorable incorporation of Eu2+ into the zircon lattice system (Trail et al., 2012).

5.4. Cu-Au Mineralization of Danyore Valley and Implications for Future Exploration

The composition of chalcopyrite in any particular ore system is primarily dependent on the existence or non-existence of various other co-crystallizing sulfides (George et al., 2016). Chalcopyrite exhibits crystallization within a body-centered tetragonal lattice system, where copper, sulfur (S), and iron (Fe) atoms are arranged in tetrahedral coordination (Li et al., 2013; Mikhlin et al., 2005; Todd et al., 2003). Previous studies (Cabri et al., 1985; Harris et al., 1992) have documented that chalcopyrite expresses extraordinary compatibility with solid solutions of Au and Ag. Numerous previous studies have highlighted the favorable hosting capabilities of chalcopyrite for various trace elements incorporated into its structure. Due to this characteristic, the trace element chemistry of chalcopyrite is a valuable tool for interpreting the formation of hydrothermal liquids in various geological settings (Barker et al., 2009; Farhan et al., 2023; Ingham et al., 2014). In the context of chalcopyrite lattice, elements including Ag, As, Co, Au, Ni, Pb, Se, Te, and S can potentially replace S and Fe atoms (George et al., 2015; George et al., 2017). Silver (Ag), gold (Au), arsenic (As), and selenium (Se) are commonly documented as trace components forming solid solutions within the chalcopyrite structure. Conversely, elements such as indium (In), thallium (Ti), gallium (Ga), and mercury (Hg) are rarely mentioned (Brill, 1989; Demir, 2008; Demir et al., 2013; George et al., 2018; Helmy et al., 2013; Huston et al., 2010; Moggi et al., 2002; Reich et al., 2020; Sadati et al., 2016; Wang et al., 2016).

Similarly, the analyzed chalcopyrites from Danyore Valley prospect host significant contents of As, Ag, Au, Cd, Sb, and Te elements, whereas Ti, Ga, Hg, and In are rare or below the detection limit. Gold (Au) was the dominant trace element discovered in the studied chalcopyrite grains, with some

Preprints.org (www.preprints.org) | NOT PEER-REVIEWED | Posted: 13 May 2024 doi:10.20944/preprints202405.0851.v1

individual grains having notable concentrations up to 1200 parts per million. Other metals are commonly present at > 400 ppm.

The integration of trace elements like Fe, Ag, Au, Cu, and Zn into the chalcopyrite composition is more intricate compared to the other typical base-metal sulfides (George et al., 2016). Selenium and Tellurium are important gold carriers because they are frequently found as trace minerals in various copper-gold deposits that mainly contain gold (Cepedal et al., 2006; Ciobanu et al., 2006; Hu et al., 2006; Novoselov et al., 2015; Plotinskaya et al., 2006; Scherbarth and Spry, 2006; Vikentyev and Petrology, 2006; Voudouris, 2010). There is an enormous positive association between Au and Se and Te (Figure 16a,b) implying the episode of Au-tellurides and selenides inclusions. Several studies (Cooke and McPhail, 2001; Seward, 1973) indicated that valuable metals were probably carried through tellurium components, shown by the strong interactions between Te, Ag, and Au (Figure 16c). In addition, Figure 16d,e demonstrate a solid positive relationship between Cu, Ag, and Au. Furthermore, the same relationship is noticed between Sb and Zn, Sb and Ag, As and Ag. Figures 16f–i suggest a moderate to strong correlation between Sb and Zn, and As and Au. In terms of a substantial positive affiliation between Te and Au contents, the Danyore Valley chalcopyrite is closely similar to Kaldom Gol chalcopyrite (Farhan et al., 2023) and the Cayeli deposit Turkey chalcopyrite (Revan et al., 2014).

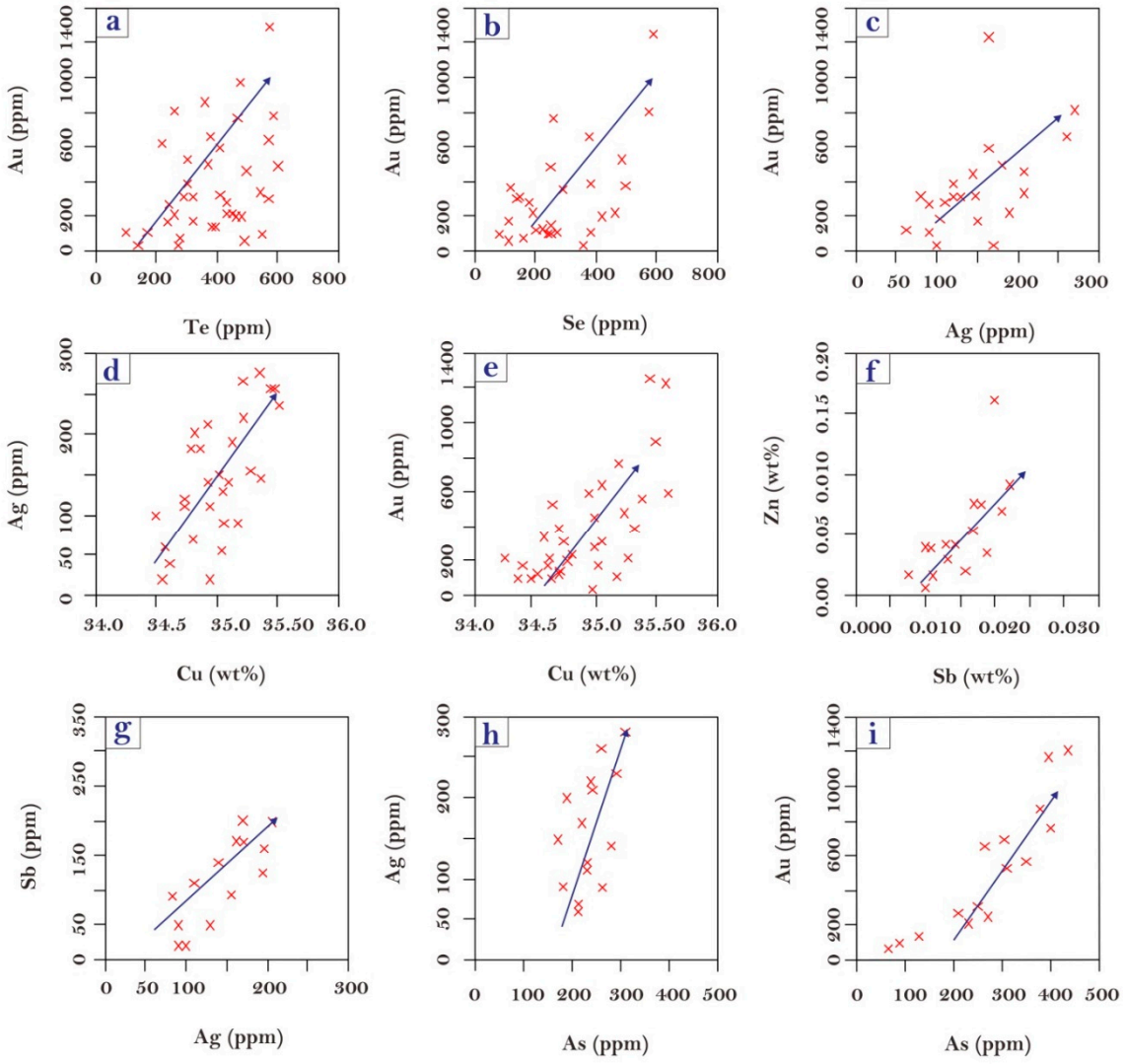

Figure 16. Binary plots illustrating the correlations among selected trace elements of chalcopyrite from the Danyore Valley copper prospect, Northern Pakistan.

Preprints.org (www.preprints.org) | NOT PEER-REVIEWED | Posted: 13 May 2024 doi:10.20944/preprints202405.0851.v1

Based on the fieldwork and microscopic studies, two types of veins have been discovered in the research area (Figure 17). The initial one is mineralized quartz veins which contain high concentrations of sulfides, surrounded by different types of alteration assemblages including chlorite, muscovite, biotite, and sericite (Figure 17a,b). The second one is late-stage barren calcite veins, which intruded on the early-stage preexisting mineralized quartz veins. This type is primarily associated with the carbonatization process (Figure 17c). The tectonic and structural setting of the region played an essential role in their formation. The gabbro-diorite host units were deformed and several cracks, fractures, and fault plans were formed within the wall rock body that allowed the metal-bearing fluids to ascend (Figure 17a,b). The ascending hydrothermal fluids rich in sulfides, filled these structure with undeformed quartz veins. Secondary carbonate minerals (i.e., malachite) and hydrothermal alterations (biotite-muscovite-chlorite-sericite zone) are formed close to these veins. A new calcic hydrothermal solution (rich in carbonate minerals) intrudes into the preexisting quartz veins. As a result, a barren calcite vein is formed, which mainly involves sulfide and quartz grains (Figure 17c).

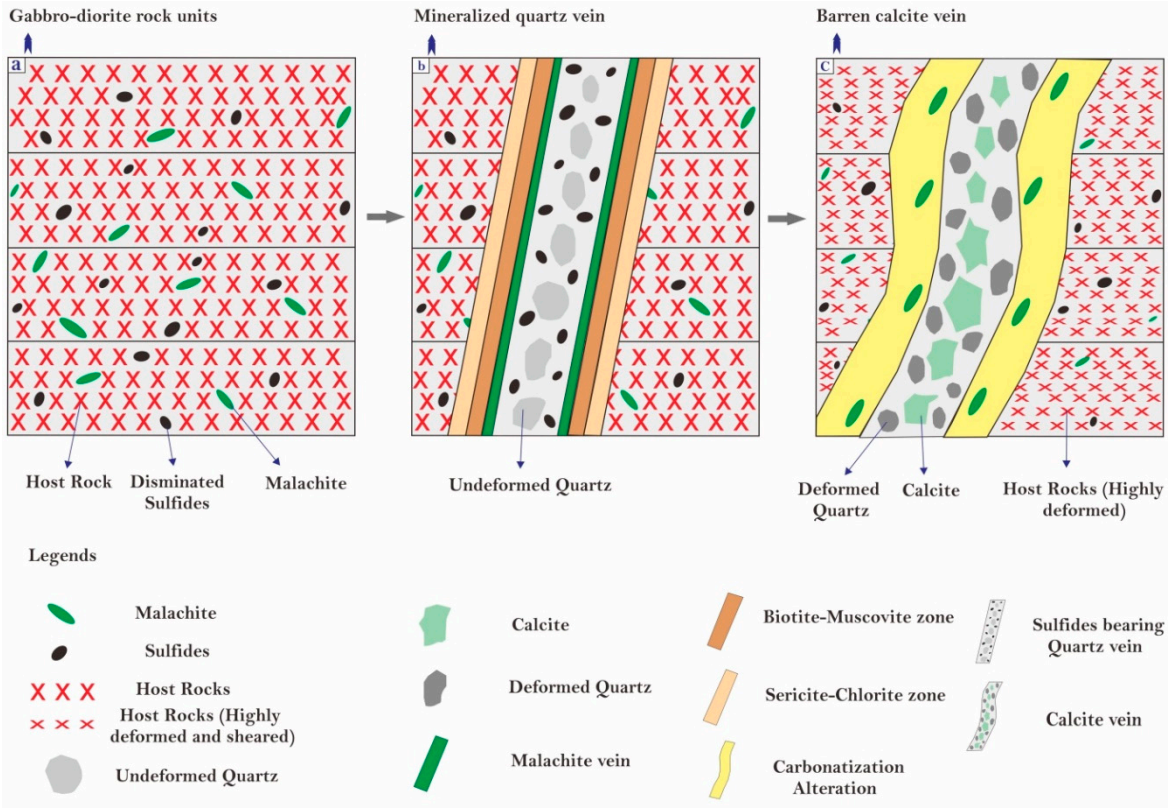

Figure 17. Two types of veins are identified in the Danyore Valley copper prospect, Northern Pakistan: (a) wall rock containing sulfides and malachite; (b) fracture system filled with mineralized quartz vein associated with the formation of malachite and alteration assemblages (biotite-muscovite and sericite-chlorite); (c) pre-existing quartz vein intruded by late-stage barren calcite vein which associated with carbonatization alteration.

The high assemblages of base and valuable metals in the analyzed specimens from Danyore Valley associated with the significant exposure of copper enrichment patterns and the field's alteration zones can be used as clues for further geological, geochemical, and geophysical studies and prospecting. The scarcity of detailed geological, structural, and geochemical data and advanced isotope analyses in the literature underscores the need for more comprehensive studies. The primary knowledge gained from the current research can serve as a foundation for understanding the Northern Pakistan region's broader geological and tectonic context and the Kohistan Batholith specifically. In addition, further mineral exploration and subsequent mining activities in the Kohistan

Preprints.org (www.preprints.org) | NOT PEER-REVIEWED | Posted: 13 May 2024 doi:10.20944/preprints202405.0851.v1

Batholith can provide substantial economic opportunities for local communities in Northern Pakistan.

6. Conclusions

The Danyore Valley area, which is located in the Kohistan Batholith, hosts several mineralized quartz veins associated with gabbro-diorite intrusions. The host bodies of Danyore Valley consist mainly of diorites and gabbros which intruded during the Early Cretaceous period (~110 Ma).

The primary magma source for the diorites and gabbros of the Danyore Valley area was derived from a depleted mantle that experienced partial metasomatization due to fluids originating from subducted slabs. The wall rock units of Danyore Valley Cu-Au prospect are most likely formed in a continental margin environment and from the same magma through fractional crystallization.

The mineralization style is characterized by sulfide-bearing quartz veins which are principally enriched in copper and gold and surrounded by sericitization, chloritization, and carbonatization. The alteration zones, sulfide mineral chemistry, and ore assemblage and textures suggested an intermediate sulfidation epithermal type of mineralization.

Future geological studies in the Danyore Valley and surrounding areas should focus on gaining a deeper understanding of the region's geological processes, mineralization mechanisms, and geodynamic history.

Supplementary Materials: The following supporting information can be downloaded at the website of this paper posted on Preprints.org. Supplementary Data Material I: Includes the analytical techniques and processes used in this study: (a) LA-ICP-MS zircon U-Pb isotope analysis for U-Pb age dating (b) X-ray fluorescence (XRF) for whole-rock geochemical studies and (c) electron probe micro-analysis (EPMA) for mineral analysis. Supplementary Data Table SI: LA-ICP-MS zircon U–Pb analytical results for gabbro-diorite samples from Danyore Valley copper prospect, Northern Pakistan. Supplementary Data Table SII: Trace element compositions (in parts per million) of studied zircon crystals for gabbro-diorite samples from Danyore Valley copper prospect, Northern Pakistan. Supplementary Data Table SIII: Chemical compositions for major, trace, and rare earth elements of analyzed samples from Danyore Valley and previous work (Heuberger et al., 2007).

Acknowledgments: The following organizations provided funding for this study: the Science and Technology Innovation Program of Hunan Province (No. 2021RC4055, No. 2022RC1182), the National Natural Science Foundation of China (No. 92162103), and the Natural Science Foundation of Hunan Province (No. 2022JJ30699, No. 2023JJ10064). The authors express gratitude to Mr. Sajid Ali (University of Potsdam, Germany) for assistance in fieldwork and making geological maps using ArcGIS. We are particularly thankful to Mr. Masroor Alam and Mohammad Azam (KIU, Pakistan) for their support during the fieldwork.

References

Ahmad, L., Khan, S.D., Tahir Shah, M., Jehan, N.J.A.J.o.G., 2018. Gold mineralization in bubin area, Gilgit-Baltistan, northern areas, Pakistan. 11, 1-12.

Alam, M., Li, S.-R., Santosh, M., Zafar, T., Hussain, Z., Yuan, M.-W., Khan, H.J.J.o.G.E., 2023. Characteristics, provenance, ore genesis and exploration of the Shimshal Valley placer gold deposits in the Karakoram Block, North Pakistan. 245, 107128.

Alam, M., Li, S.R., Santosh, M., Yuan, M.W.J.G.J., 2019. Morphology and chemistry of placer gold in the Bagrote and Dainter streams, northern Pakistan: Implications for provenance and exploration. 54, 1672-1687.

Anczkiewicz, 2000. Isotopic constraints on the evolution of metamorphic conditions in the Jijal-Patan complex and the Kamila Belt of the Kohistan arc, Pakistan Himalaya. 170, 321-331.

Arndt, N., Lesher, C., Czamanske, G., 2005. Mantle-derived magmas and magmatic Ni-Cu-(PGE) deposits.

Ashraf, 1999. Structural geology of the western extremity of the kohistan island arc. 71.

Auden, J.J.R.o.G.s.o.I., 1935. Traverses in the Himalaya. 69, 123-167.

Ayonta Kenne, P., Tanko Njiosseu, E.L., Ganno, S., Ngnotue, T., Fossi, D.H., Hamdja Ngoniri, A., Nga Essomba, P., Nzenti, J.P.J.G.J., 2021. Zircon trace element geochemistry and Ti-in-zircon thermometry of the Linté Pan-African granitoids, Central Cameroon: Constraints on the genesis of host magma and tectonic implications. 56, 4830-4848.

Ballard, J.R., Palin, J.M., Campbell, I.H.J.C.t.M., Petrology, 2002. Relative oxidation states of magmas inferred from Ce (IV)/Ce (III) in zircon: application to porphyry copper deposits of northern Chile. 144, 347-364.

Bao, Z., Sun, W., Li, C., Zhao, Z.J.O.G.R., 2014. U–Pb dating of hydrothermal zircon from the Dongping gold deposit in North China: constraints on the mineralization processes. 61, 107-119.

Preprints.org (www.preprints.org) | NOT PEER-REVIEWED | Posted: 13 May 2024 doi:10.20944/preprints202405.0851.v1

Barker, S.L., Hickey, K.A., Cline, J.S., Dipple, G.M., Kilburn, M.R., Vaughan, J.R., Longo, A.A.J.E.G., 2009. Uncloaking invisible gold: Use of nanoSIMS to evaluate gold, trace elements, and sulfur isotopes in pyrite from Carlin-type gold deposits. 104, 897-904.

Barth, A.P., Wooden, J.L.J.C.G., 2010. Coupled elemental and isotopic analyses of polygenetic zircons from granitic rocks by ion microprobe, with implications for melt evolution and the sources of granitic magmas. 277, 149-159.

Bignold, S.M., Treloar, P.J., Petford, N.J.C.G., 2006. Changing sources of magma generation beneath intra-oceanic island arcs: an insight from the juvenile Kohistan island arc, Pakistan Himalaya. 233, 46-74.

Bignold, S.T., Journal of the Geological Society, 2003. Northward subduction of the Indian Plate beneath the Kohistan island arc, Pakistan Himalaya: new evidence from isotopic data. 160, 377-384.

Boynton, W.V., 1984. Cosmochemistry of the rare earth elements: meteorite studies, Developments in geochemistry. Elsevier, pp. 63-114.

Brill, B.A.J.T.C.M., 1989. Trace-element contents and partitioning of elements in ore minerals from the CSA Cu-Pb-Zn deposit, Australia, and implications for ore genesis. 27, 263-274.

Briqueu, L., Bougault, H., Joron, J.L.J.E., Letters, P.S., 1984. Quantification of Nb, Ta, Ti and V anomalies in magmas associated with subduction zones: petrogenetic implications. 68, 297-308.

Brown, G., Thorpe, R., Webb, P.J.J.o.t.G.S., 1984. The geochemical characteristics of granitoids in contrasting arcs and comments on magma sources. 141, 413-426.

Bukhari, Syed Hussain, 2010, P.W.G.C., 2010. Country Update Paper on Pakistan.

Burg, J.P., Jagoutz, O., Dawood, H., Hussain, S.S.J.T., 2006. Precollision tilt of crustal blocks in rifted island arcs: Structural evidence from the Kohistan Arc. 25.

Burnham, A.D., Berry, A.J.J.G.e.C.A., 2012. An experimental study of trace element partitioning between zircon and melt as a function of oxygen fugacity. 95, 196-212.

Cabri, L.J., Campbell, J.L., Laflamme, J.G., Leigh, R.G., Maxwell, J.A., Scott, J.D.J.T.C.M., 1985. Proton-microprobe analysis of trace elements in sulfides from some massive-sulfide deposits. 23, 133-148.

Calkins, J.A., Jamiluddin, S., Bhuyan, K., Hussain, A., 1981. Geology and mineral resources of the Chitral-Partsan area, Hindu Kush Range, northern Pakistan. US Govt. Print. Off.; for sale by the Distribution Branch, US Geological ….

Candela, P.A., Piccoli, P.M., 2005. Magmatic processes in the development of porphyry-type ore systems.

Carley, T.L., Miller, C.F., Wooden, J.L., Padilla, A.J., Schmitt, A.K., Economos, R.C., Bindeman, I.N., Jordan, B.T.J.E., Letters, P.S., 2014. Iceland is not a magmatic analog for the Hadean: Evidence from the zircon record. 405, 85-97.

Cepedal, A., Fuertes-Fuente, M., Martin-Izard, A., Gonzalez-Nistal, S., Rodriguez-Pevida, L.J.M., Petrology, 2006. Tellurides, selenides and Bi-mineral assemblages from the Río Narcea Gold Belt, Asturias, Spain: genetic implications in Cu–Au and Au skarns. 87, 277-304.

Chappell, B.W., White, A.J.E., Edinburgh, E.S.T.o.t.R.S.o., 1992. I-and S-type granites in the Lachlan Fold Belt. 83, 1-26.

Chiaradia, M.J.N.C., 2020. Gold endowments of porphyry deposits controlled by precipitation efficiency. 11, 248.

Ciobanu, C., Cook, N., Damian, F., Damian, G.J.M., Petrology, 2006. Gold scavenged by bismuth melts: An example from Alpine shear-remobilizates in the Highiş Massif, Romania. 87, 351-384.

Claiborne, L.L., Miller, C.F., Flanagan, D.M., Clynne, M.A., Wooden, J.L.J.G., 2010. Zircon reveals protracted magma storage and recycling beneath Mount St. Helens. 38, 1011-1014.

Cooke, D.R., McPhail, D.J.E.G., 2001. Epithermal Au-Ag-Te mineralization, Acupan, Baguio district, Philippines: numerical simulations of mineral deposition. 96, 109-131.

Coward, M., Butler, R., Khan, M.A., Knipe, R.J.J.o.t.G.S., 1987. The tectonic history of Kohistan and its implications for Himalayan structure. 144, 377-391.

Danishwar, S., Stern, R., Khan, M.J.J.o.A.E.S., 2001. Field relations and structural constraints for the Teru volcanic formation, northern Kohistan Terrane, Pakistani Himalayas. 19, 683-695.

Demir, 2008. Mineralogy, mineral chemistry, and fluid inclusion investigation of Köstere hydrothermal vein-type deposit (Gümüşhane, NE-Turkey).

Demir, Y., Uysal, İ., Sadıklar, M.J.O.G.R., 2013. Mineral chemical investigation on sulfide mineralization of the Istala deposit, Gümüşhane, NE-Turkey. 53, 306-317.

Dhuime, B., Bosch, D., Bodinier, J.-L., Garrido, C., Bruguier, O., Hussain, S.S., Dawood, H.J.E., Letters, P.S., 2007. Multistage evolution of the Jijal ultramafic–mafic complex (Kohistan, N Pakistan): implications for building the roots of island arcs. 261, 179-200.

Faisal, M., Yang, X., Khalifa, I.H., Amuda, A.K., Sun, C.J.P.R., 2020. Geochronology and geochemistry of Neoproterozoic Hamamid metavolcanics hosting largest volcanogenic massive sulfide deposits in Eastern Desert of Egypt: Implications for petrogenesis and tectonic evolution. 344, 105751.

Farhan, M., Arif, M., Ye, Y., Li, C.-F., Chen, X., Garbe-Schönberg, D., Wu, T., Ullah, Z., Hussain, Z., Zafar, T.J.G., 2023. Fluid source and physicochemical conditions of the polymetallic mineralization in Gawuch Formation, Kohistan Island Arc, NW Pakistan. 83, 125949.

Preprints.org (www.preprints.org) | NOT PEER-REVIEWED | Posted: 13 May 2024 doi:10.20944/preprints202405.0851.v1

Franklin, J., Gibson, H., Jonasson, I., Galley, A., 2005. Volcanogenic massive sulfide deposits.
Frost, B.R., Barnes, C.G., Collins, W.J., Arculus, R.J., Ellis, D.J., Frost, C.D.J.J.o.p., 2001. A geochemical classification for granitic rocks. 42, 2033-2048.
Frost, D.J., McCammon, C.A.J.A.R.E.P.S., 2008. The redox state of Earth's mantle. 36, 389-420.
Gaetani, G.A., Grove, T.L.J.C.t.M., Petrology, 1998. The influence of water on melting of mantle peridotite. 131, 323-346.
Garwin, S.J.A.E.A., 2019. The geological characteristics, geochemical signature and geophysical expression of porphyry copper-(gold) deposits in the circum-Pacific region. 2019, 1-4.
Geng, H., Sun, M., Yuan, C., Zhao, G., Xiao, W.J.J.o.A.E.S., 2011. Geochemical and geochronological study of early Carboniferous volcanic rocks from the West Junggar: petrogenesis and tectonic implications. 42, 854-866.
George, L., Cook, N.J., Ciobanu, C.L., 2015. Trace element partitioning between co-existing sphalerite, galena and chalcopyrite, pp. 737-740.
George, L.L., Cook, N.J., Ciobanu, C.L.J.M., 2017. Minor and trace elements in natural tetrahedrite-tennantite: Effects on element partitioning among base metal sulphides. 7, 17.
George, L.L., Cook, N.J., Ciobanu, C.L.J.O.G.R., 2016. Partitioning of trace elements in co-crystallized sphalerite–galena–chalcopyrite hydrothermal ores. 77, 97-116.
George, L.L., Cook, N.J., Crowe, B.B., Ciobanu, C.L.J.M.M., 2018. Trace elements in hydrothermal chalcopyrite. 82, 59-88.
Gill, J.B., Gill, J.B.J.O.A., Tectonics, P., 1981. Andesite Magmas, Ejecta, Eruptions, and Volcanoes. 64-96.
Goldfarb, R.J., Baker, T., Dubé, B., Groves, D.I., Hart, C.J., Gosselin, P., 2005. Distribution, character, and genesis of gold deposits in metamorphic terran.
Griesbach, C.J.R.G.S.I., 1893. Notes on the Central Himalaya. 26, 19-25.
Grimes, C.B., John, B.E., Cheadle, M.J., Mazdab, F.K., Wooden, J.L., Swapp, S., Schwartz, J.J.J.C.t.M., Petrology, 2009. On the occurrence, trace element geochemistry, and crystallization history of zircon from in situ ocean lithosphere. 158, 757-783.
Grimes, C.B., John, B.E., Kelemen, P., Mazdab, F., Wooden, J., Cheadle, M.J., Hanghøj, K., Schwartz, J.J.G., 2007. Trace element chemistry of zircons from oceanic crust: A method for distinguishing detrital zircon provenance. 35, 643-646.
Hamidullah, S., Jan, M.Q.J.G.B.U.o.P., 1986. Preliminary petrochemical study of the Chilas complex, Kohistan island arc, northern Pakistan. 19, 157-182.
Harris, N., Inger, S.J.C.t.M., Petrology, 1992. Trace element modelling of pelite-derived granites. 110, 46-56.
Helmy, H., Ballhaus, C., Fonseca, R., Nagel, T.J.C.t.M., Petrology, 2013. Fractionation of platinum, palladium, nickel, and copper in sulfide–arsenide systems at magmatic temperature. 166, 1725-1737.
Heuberger, S., Schaltegger, U., Burg, J.-P., Villa, I.M., Frank, M., Dawood, H., Hussain, S., Zanchi, A.J.S.J.o.G., 2007. Age and isotopic constraints on magmatism along the Karakoram-Kohistan Suture Zone, NW Pakistan: Evidence for subduction and continued convergence after India-Asia collision. 100, 85-107.
Hoskin, P.W., Schaltegger, U.J.R.i.m., geochemistry, 2003. The composition of zircon and igneous and metamorphic petrogenesis. 53, 27-62.
Hoskin, P.W.J.G.e.c.a., 2005. Trace-element composition of hydrothermal zircon and the alteration of Hadean zircon from the Jack Hills, Australia. 69, 637-648.
Hou, Z., Cook, N.J.J.O.G.R., 2009. Metallogenesis of the Tibetan collisional orogen: A review and introduction to the special issue. 36, 2-24.
Hu, M.-S., Chen, H.-L., Shen, C.-H., Hong, L.-S., Huang, B.-R., Chen, K.-H., Chen, L.-C.J.N.m., 2006. Photosensitive gold-nanoparticle-embedded dielectric nanowires. 5, 102-106.
Hussain, A., Zhao, K.-D., Arif, M., Palmer, M.R., Chen, W., Zhang, Q., Li, Q., Jiang, S.-Y., Girei, M.B.J.O.G.R., 2020. Geochronology, mineral chemistry and genesis of REE mineralization in alkaline rocks from the Kohistan Island Arc, Pakistan. 126, 103749.
Hussain, Z., Tao, C., Li, C.-F., Liao, S., Alam, M., Farhan, M., Zhang, H., Hussain, A.J.M., 2021. Mineralogy, Fluid Inclusions, and Isotopic Study of the Kargah Cu-Pb Polymetallic Vein-Type Deposit, Kohistan Island Arc, Northern Pakistan: Implication for Ore Genesis. 11, 1266.
Hussain, Z., Zhang, C.-L., Sargazi, M., Song, Z.-H., Farhan, M., Alam, M., Hussain, S.A., Ullah, Z., Hussain, A., Sadiq, I.J.O.G.R., 2023. Fluid provenance and genetic type of the Bubin Cu-Pb polymetallic deposit, Kohistan-Ladakh island arc, north Pakistan: Evidence from mineralogy, fluid inclusion and ohs-pb isotopes. 105776.
Huston, D.L., Pehrsson, S., Eglington, B.M., Zaw, K.J.E.G., 2010. The geology and metallogeny of volcanic-hosted massive sulfide deposits: Variations through geologic time and with tectonic setting. 105, 571-591.
Ingham, E.S., Cook, N.J., Cliff, J., Ciobanu, C.L., Huddleston, A.J.G.e.C.A., 2014. A combined chemical, isotopic and microstructural study of pyrite from roll-front uranium deposits, Lake Eyre Basin, South Australia. 125, 440-465.

Preprints.org (www.preprints.org) | NOT PEER-REVIEWED | Posted: 13 May 2024 doi:10.20944/preprints202405.0851.v1

Irvine, T.N., Baragar, W.J.C.j.o.e.s., 1971. A guide to the chemical classification of the common volcanic rocks. 8, 523-548.

Jagoutz, O.E., Burg, J.-P., Hussain, S., Dawood, H., Pettke, T., Iizuka, T., Maruyama, S.J.C.t.M., Petrology, 2009. Construction of the granitoid crust of an island arc part I: geochronological and geochemical constraints from the plutonic Kohistan (NW Pakistan). 158, 739-755.

Jan, M.Q., Howie, R.J.J.o.P., 1981. The mineralogy and geochemistry of the metamorphosed basic and ultrabasic rocks of the Jijal complex, Kohistan, NW Pakistan. 22, 85-126.

Jan, M.Q., Tahirkheli, R.J.G.B.P.U., 1979. Petrography of the amphibolites of Swat and Kohistan. 11, 51-64.

Jan, M.Q., Windly, BRIAN F %J Journal of Petrology, 1990. Chromian spinel-silicate chemistry in ultramafic rocks of the Jijal complex, Northwest Pakistan. 31, 667-715.

Kazmi, A.H., Jan, M.Q.J., 1997. Geology and tectonics of Pakistan.

Kerrich, R., Goldfarb, R., Groves, D., Garwin, S., Jia, Y.J.S.i.C.S.D.E.S., 2000. The characteristics, origins, and geodynamic settings of supergiant gold metallogenic provinces. 43, 1-68.

Kerrich, R., Goldfarb, R.J., Richards, J.P., 2005. Metallogenic provinces in an evolving geodynamic framework.

Kesler, S.E., Chryssoulis, S.L., Simon, G.J.O.G.R., 2002. Gold in porphyry copper deposits: its abundance and fate. 21, 103-124.

Khan, M.A., Bhattarai, A., Kuznia, J., Olson, D.J.A.P.L., 1993. High electron mobility transistor based on a GaN-Al x Ga1− x N heterojunction. 63, 1214-1215.

Khan, M.A., Treloar, P.J., Khan, M.A., Khan, T., Qazi, M.S., Jan, M.Q.J.J.o.A.E.S., 1998. Geology of the Chalt–Babusar transect, Kohistan terrane, N. Pakistan: implications for the constitution and thickening of island-arc crust. 16, 253-268.

Khan, S.D., Walker, D.J., Hall, S.A., Burke, K.C., Shah, M.T., Stockli, L.J.G.S.o.A.B., 2009. Did the Kohistan-Ladakh island arc collide first with India? 121, 366-384.

Khan Tehseenullah, A.K., M, Qasim Jan, M., Naseem, M.J.G.A., 1996. Back-arc basin assemblages in Kohistan, Northern Pakistan. 9, 30-40.

Kirkland, C., Smithies, R., Taylor, R., Evans, N., McDonald, B.J.L., 2015. Zircon Th/U ratios in magmatic environs. 212, 397-414.

Li, J.-X., Qin, K.-Z., Li, G.-M., Richards, J.P., Zhao, J.-X., Cao, M.-J.J.L., 2014. Geochronology, geochemistry, and zircon Hf isotopic compositions of Mesozoic intermediate–felsic intrusions in central Tibet: Petrogenetic and tectonic implications. 198, 77-91.

Li, Y., Kawashima, N., Li, J., Chandra, A., Gerson, A.R.J.A.i.c., science, i., 2013. A review of the structure, and fundamental mechanisms and kinetics of the leaching of chalcopyrite. 197, 1-32.

Ludwig, 2008. User's manual for IsoPlot 3.0. 71.

Ma, L., Li, N., Guo, Y., Wang, X., Yang, S., Huang, M., Zhang, H.J.I.T.o.C., 2021. Learning to optimize: reference vector reinforcement learning adaption to constrained many-objective optimization of industrial copper burdening system.

Malkani, M.S., Buzdar, M.A., Khosa, M.H., Kakar, A.S., Saeed, F., Alyani, M.I., 2019. Closure of Tethys Sea and Paleo Vitakri River systems, and the birth of Paleo Indus River systems in Pakistan; Geodynamic and Geobiological Evolution of Indo-Pak subcontinent (South Asia).

McCulloch, M.T., Gamble, J.J.E., Letters, P.S., 1991. Geochemical and geodynamical constraints on subduction zone magmatism. 102, 358-374.

McDonough, W.F., Sun, S.-S.J.C.g., 1995. The composition of the Earth. 120, 223-253.

McMahon, C.J.R.G.S.o.I., 1884. Microscopic structures of some Himalayan granites and gneissose granites. 17, 53-73.

Miandad, S., Shah, M.T., Khan, S.D., Ahmad, L.J.J.o.H.E.S., 2014. Investigation for gold and base metals mineralization and petrochemical characteristics of the rocks of upper parts of Bagrot valley, Gilgit-Baltistan, Pakistan. 47, 29.

Mikhlin, Y., Tomashevich, Y., Tauson, V., Vyalikh, D., Molodtsov, S., Szargan, R.J.J.o.E.S., Phenomena, R., 2005. A comparative X-ray absorption near-edge structure study of bornite, Cu5FeS4, and chalcopyrite, CuFeS2. 142, 83-88.

Moggi, Cecchi, V., Cipriani, C., Rossi, P., Ceccato, D., Rudello, V., Somacal, H.J.P.d.M., 2002. Trace element contents and distribution maps of chalcopyrite: a micro-PIXE study. 71, 101-109.

Molnar, P., Atwater, T., Mammerickx, J., Smith, S.M.J.G.J.I., 1975. Magnetic anomalies, bathymetry and the tectonic evolution of the South Pacific since the Late Cretaceous. 40, 383-420.

Novoselov, K., Belogub, E., Kotlyarov, V., Mikhailov, A.J.E.J.o.M., 2015. Ore mineralogy and formation conditions of the Pirunkoukku gold occurrence (Finland). 27, 639-649.

Pearce, J.A., Harris, N.B., Tindle, A.G.J.J.o.p., 1984. Trace element discrimination diagrams for the tectonic interpretation of granitic rocks. 25, 956-983.

Pearce, N.J., Perkins, W.T., Westgate, J.A., Gorton, M.P., Jackson, S.E., Neal, C.R., Chenery, S.P.J.G.n., 1997. A compilation of new and published major and trace element data for NIST SRM 610 and NIST SRM 612 glass reference materials. 21, 115-144.

Preprints.org (www.preprints.org) | NOT PEER-REVIEWED | Posted: 13 May 2024 doi:10.20944/preprints202405.0851.v1

Petterson, M., Windley, B.J.E., Letters, P.S., 1991. Changing source regions of magmas and crustal growth in the Trans-Himalayas: evidence from the Chalt volcanics and Kohistan batholith, Kohistan, northern Pakistan. 102, 326-341.

Petterson, M.G., Windley, B.F.J.E., Letters, P.S., 1985. RbSr dating of the Kohistan arc-batholith in the Trans-Himalaya of north Pakistan, and tectonic implications. 74, 45-57.

Petterson, M.G.J.G.S., London, Special Publications, 2010. A review of the geology and tectonics of the Kohistan island arc, north Pakistan. 338, 287-327.

Pettke, T., Audétat, A., Schaltegger, U., Heinrich, C.A.J.C.G., 2005. Magmatic-to-hydrothermal crystallization in the W–Sn mineralized Mole Granite (NSW, Australia): Part II: Evolving zircon and thorite trace element chemistry. 220, 191-213.

Plotinskaya, O.Y., Kovalenker, V., Seltmann, R., Stanley, C.J.M., Petrology, 2006. Te and Se mineralogy of the high-sulfidation Kochbulak and Kairagach epithermal gold telluride deposits (Kurama Ridge, Middle Tien Shan, Uzbekistan). 87, 187-207.

Pudsey, C.J.J.G.M., 1986. The Northern Suture, Pakistan: margin of a Cretaceous island arc. 123, 405-423.

Raza, M.Q., Absar, N., Pandalai, H., Patel, S.J.O.G.R., 2021. Chlorite thermometry and fluid inclusion studies on vein-type Tintini copper deposit, Eastern Dharwar Craton, India: Ore genetic implications. 131, 104058.

Reich, M., Román, N., Barra, F., Morata, D.J.M., 2020. Silver-rich chalcopyrite from the active Cerro Pabellón geothermal system, northern Chile. 10, 113.

Revan, M.K., Genç, Y., Maslennikov, V.V., Maslennikova, S.P., Large, R.R., Danyushevsky, L.V.J.O.G.R., 2014. Mineralogy and trace-element geochemistry of sulfide minerals in hydrothermal chimneys from the Upper-Cretaceous VMS deposits of the eastern Pontide orogenic belt (NE Turkey). 63, 129-149.

Robertson, A.H., Collins, A.S.J.J.o.A.E.S., 2002. Shyok Suture Zone, N Pakistan: late Mesozoic–Tertiary evolution of a critical suture separating the oceanic Ladakh Arc from the Asian continental margin. 20, 309-351.

Rolland, Y., Mahéo, G., Pecher, A., Villa, I.M.J.J.o.A.E.S., 2009. Syn-kinematic emplacement of the Pangong metamorphic and magmatic complex along the Karakorum Fault (N Ladakh). 34, 10-25.

Rubatto, Daniela, mineralogy, J.R.i., geochemistry, 2017. Zircon: the metamorphic mineral. 83, 261-295.

Sadati, S.N., Yazdi, M., Mao, J., Behzadi, M., Adabi, M.H., Lingang, X., Zhenyu, C., Mokhtari, M.A.A.J.O.G.R., 2016. Sulfide mineral chemistry investigation of sediment-hosted stratiform copper deposits, Nahand-Ivand area, NW Iran. 72, 760-776.

Schaltegger, U., Brack, P., Ovtcharova, M., Peytcheva, I., Schoene, B., Stracke, A., Marocchi, M., Bargossi, G.M.J.E., Letters, P.S., 2009. Zircon and titanite recording 1.5 million years of magma accretion, crystallization and initial cooling in a composite pluton (southern Adamello batholith, northern Italy). 286, 208-218.

Schaltegger, U., Zeilinger, G., Frank, M., Burg, J.P.J.T.n., 2002. Multiple mantle sources during island arc magmatism: U–Pb and Hf isotopic evidence from the Kohistan arc complex, Pakistan. 14, 461-468.

Scherbarth, N.L., Spry, P.G.J.E.G., 2006. Mineralogical, petrological, stable isotope, and fluid inclusion characteristics of the Tuvatu gold-silver telluride deposit, Fiji: Comparisons with the Emperor deposit. 101, 135-158.

Searle, M., Khan, M.A., Fraser, J., Gough, S., Jan, M.Q.J.T., 1999. The tectonic evolution of the Kohistan-Karakoram collision belt along the Karakoram Highway transect, north Pakistan. 18, 929-949.

Searle, M., Windley, B., Coward, M., Cooper, D., Rex, A., Rex, D., Tingdong, L., Xuchang, X., Jan, M., Thakur, V.J.G.S.o.A.B., 1987. The closing of Tethys and the tectonics of the Himalaya. 98, 678-701.

Seltmann, R., Faragher, A., Kämpf, H., Moeller, P., 1994. Collisional orogens and their related metallogeny-a preface, Metallogeny of Collisional Orogens.

Seward, H.H., 1973. Measuring user satisfaction to evaluate information systems. Harvard University.

Shah, M., Khan, S., Tahirkheli, T., Ahmad, L., Miandad, S., Rehman, A., Ali, L., 2012. Prospects of gold mineralization in the Gilgit-Baltistan Province of Pakistan, pp. NS23A-1650.

Shah, M.T., Shervais, J.W.J.J.o.A.E.S., 1999. The Dir-Utror metavolcanic sequence, Kohistan arc terrane, northern Pakistan. 17, 459-475.

Shand, S.J.J.B.o.t.G.S.o.A., 1942. Phase petrology in the Cortlandt complex, New York. 53, 409-428.

Sibuet, J.C., Srivastava, S.P., Spakman, W.J.J.o.G.R.S.E., 2004. Pyrenean orogeny and plate kinematics. 109.

Sillitoe, R.H.J.E.g., 2010. Porphyry copper systems. 105, 3-41.

Sláma, J., Košler, J., Condon, D.J., Crowley, J.L., Gerdes, A., Hanchar, J.M., Horstwood, M.S., Morris, G.A., Nasdala, L., Norberg, N.J.C.G., 2008. Plešovice zircon—a new natural reference material for U–Pb and Hf isotopic microanalysis. 249, 1-35.

Sullivan, M.A., 1992. The geology of the roof-zone of the Kohistan batholith, northwestern Pakistan. University of Leicester (United Kingdom).

Sylvester, P.J.J.l., 1998. Post-collisional strongly peraluminous granites. 45, 29-44.

Tahirkheli, R.A.J.G.B.U.P., 1979. Geology of kohistan, karakoram, himalaya, northern. 11, 1-30.

Tahirkheli, R.K., Jan, Q., 1984. The geographical and geological domains on the Karakoram, pp. 57-70.

Preprints.org (www.preprints.org) | NOT PEER-REVIEWED | Posted: 13 May 2024 doi:10.20944/preprints202405.0851.v1

Tahirkheli, T., Shah, M.T., Khan, M.A., Bilqees, R.J.J.o.H.E.S., 2012. Mineralogy and geochemistry of diorites and associated hydrothermal sulfide mineralization of Gawuch Formation in Drosh area, Chitral, northern Pakistan. 45.

Todd, E., Sherman, D., Purton, J.J.G.e.C.A., 2003. Surface oxidation of chalcopyrite (CuFeS2) under ambient atmospheric and aqueous (pH 2-10) conditions: Cu, Fe L-and O K-edge X-ray spectroscopy. 67, 2137-2146.

Trail, D., Watson, E.B., Tailby, N.D.J.G.e.C.A., 2012. Ce and Eu anomalies in zircon as proxies for the oxidation state of magmas. 97, 70-87.

Trail, D., Watson, E.B., Tailby, N.D.J.N., 2011. The oxidation state of Hadean magmas and implications for early Earth's atmosphere. 480, 79-82.

Treloar, J, P., Rex, D., Guise, P., Coward, M., Searle, M., Windley, B., Petterson, M., Jan, M., Luff, I.J.T., 1989. K-Ar and Ar-Ar geochronology of the Himalayan collision in NW Pakistan: Constraints on the timing of suturing, deformation, metamorphism and uplift. 8, 881-909.

Treloar, P.J., Petterson, M.G., Jan, M.Q., Sullivan, M.J.J.o.t.G.S., 1996. A re-evaluation of the stratigraphy and evolution of the Kohistan arc sequence, Pakistan Himalaya: implications for magmatic and tectonic arc-building processes. 153, 681-693.

Vikentyev, I.J.M., Petrology, 2006. Precious metal and telluride mineralogy of large volcanic-hosted massive sulfide deposits in the Urals. 87, 305-326.

Virdi, N., Tectonophysics, 1987. Northern margin of the Indian Plate—some litho-tectonic constraints. 134, 29-38.

Voudouris, P.J.I.L.S.i.a.t.G.-N.D.D., 2010. Gold deposits in Greece. mineralogy and genetic considerations. 10.

Wadia, D.N.J.M.G.S.I., 1928. The geology of Poonch State (Kashmir) and adjacent portions of the Punjab. 51, 185-370.

Wang, J., Tao, L., Zhao, H., Hu, M., Zheng, X., Peng, H., Gan, X., Xiao, W., Cao, P., Qin, W.J.M.E., 2016. Cooperative effect of chalcopyrite and bornite interactions during bioleaching by mixed moderately thermophilic culture. 95, 116-123.

Wiedenbeck, M., Alle, P., Corfu, F., Griffin, W.L., Meier, M., Oberli, F.v., Quadt, A.v., Roddick, J., Spiegel, W.J.G.n., 1995. Three natural zircon standards for U-Th-Pb, Lu-Hf, trace element and REE analyses. 19, 1-23.

Wilson, M., 1989. Igneous petrogenesis. Springer.

Xia, X., Sun, M., Geng, H., Sun, Y., Wang, Y., Zhao, G.J.J.o.A.A.S., 2011. Quasi-simultaneous determination of U-Pb and Hf isotope compositions of zircon by excimer laser-ablation multiple-collector ICPMS. 26, 1868-1871.

Yamamoto, H., Nakamura, E.J.G.S., London, Special Publications, 2000. Timing of magmatic and metamorphic events in the Jijal complex of the Kohistan arc deduced from Sm-Nd dating of mafic granulites. 170, 313-319.

Yin, A., Harrison, T.M.J.A.r.o.e., sciences, p., 2000. Geologic evolution of the Himalayan-Tibetan orogen. 28, 211-280.

Zanchi, Andrea, Gaetani, M.J.I.j.o.G., 2011. The geology of the Karakoram range, Pakistan: the new 1: 100,000 geological map of Central-Western Karakoram. 130, 161-262.

Zaw, K., Peters, S.G., Cromie, P., Burrett, C., Hou, Z.J.O.G.R., 2007. Nature, diversity of deposit types and metallogenic relations of South China. 31, 3-47.

Zeitler, P.K., Chamberlain, C.P.J.T., 1991. Petrogenetic and tectonic significance of young leucogranites from the northwestern Himalaya, Pakistan. 10, 729-741.

Zhang, F.-F., Wang, Y.-H., Xue, C.-J., Liu, J.-j., Zhang, W.J.O.G.R., 2019. Fluid inclusion and isotope evidence for magmatic-hydrothermal fluid evolution in the Tuwu porphyry copper deposit, Xinjiang, NW China. 113, 103078.

Zhang, K.-J.J.T., 1997. North and South China collision along the eastern and southern North China margins. 270, 145-156.

Zhao, X.-Y., Zhong, H., Hu, R.-Z., Mao, W., Bai, Z.-J., Lan, T.-G., Xue, K.J.E.G., 2021. Evolution of Multistage Hydrothermal Fluids in the Luoboling Porphyry Cu-Mo Deposit, Zijinshan Ore Field, Fujian Province, China: Insights from LA-ICP-MS Analyses of Fluid Inclusions. 116, 581-606.

Disclaimer/Publisher's Note: The statements, opinions and data contained in all publications are solely those of the individual author(s) and contributor(s) and not of MDPI and/or the editor(s). MDPI and/or the editor(s) disclaim responsibility for any injury to people or property resulting from any ideas, methods, instructions or products referred to in the content.